The FEBS Journal

FEBS PRESS science publishing by scientists

Immune sensing of mouse polyomavirus DNA by p204 and cGAS DNA sensors

Boris Ryabchenko, Irina Soldatova, Vojtech Šroller, Jitka Forstová and Sandra Huérfano

Department of Genetics and Microbiology, Faculty of Science, Charles University, Biocev, Czech Republic

Keywords
cGAS sensor; immune sensing of DNA; mouse polyomavirus; p204 sensor; pattern recognition receptors

Correspondence
S. Huérfano, Department of Genetics and Microbiology, Faculty of Science, Charles University, Biocev, Vestec 25250, Czech Republic
Tel: +420325873955
E-mail: huerfano@natur.cuni.cz

Boris Ryabchenko and Irina Soldatova contributed equally to this work.

(Received 16 March 2021, revised 20 May 2021, accepted 7 May 2021)

doi:10.1111/febs.15962

The mechanism by which DNA viruses interact with different DNA sensors and their connection with the activation of interferon (IFN) type I pathway are poorly understood. We investigated the roles of protein 204 (p204) and cyclic guanosine-adenosine synthetase (cGAS) sensors during infection with mouse polyomavirus (MPyV). The phosphorylation of IFN regulatory factor 3 (IRF3) and the stimulator of IFN genes (STING) proteins and the upregulation of IFN beta (IFN-β) and MX Dynamin Like GTPase 1 (MX-1) genes were detected at the time of replication of MPyV genomes in the nucleus. STING knockout abolished the IFN response. Infection with a mutant virus that exhibits defective nuclear entry via nucleopores and that accumulates in the cytoplasm confirmed that replication of viral genomes in the nucleus is required for IFN induction. The importance of both DNA sensors, p204 and cGAS, in MPyV-induced IFN response was demonstrated by downregulation of the IFN pathway observed in p204-knockdown and cGAS-knockout cells. Confocal microscopy revealed the colocalization of p204 with MPyV genomes in the nucleus. cGAS was found in the cytoplasm, colocalizing with viral DNA leaked from the nucleus and with DNA within micronucleus-like bodies, but also with the MPyV genomes in the nucleus. However, 2′3′-Cyclic guanosine monophosphate–adenosine monophosphate synthesized by cGAS was detected exclusively in the cytoplasm. Biochemical assays revealed no evidence of functional interaction between cGAS and p204 in the nucleus. Our results provide evidence for the complex interactions of MPyV and DNA sensors including the sensing of viral genomes in the nucleus by p204 and of leaked viral DNA and micronucleus-like bodies in the cytoplasm by cGAS.

Introduction

The Polyomaviridae family of small nonenveloped DNA tumor viruses consists of viruses that infect birds and mammals. Presently, 14 human polyomaviruses have been described [1,2]. Some, notably the BK polyomavirus (BKPyV), the JC polyomavirus (JCPyV), the Merkel cell polyomavirus (MCPyV), and the trichodysplasia spinulosa polyomavirus (TSPyV), were found to have a clear association with human diseases [3–6]. Human polyomaviruses are prevalent in the healthy population [7] and cause disease in immunosuppressed hosts. The high prevalence of polyomaviruses in the healthy population suggests that these viruses modulate the immune response to keep low levels of replication in favor of persistence [8–10].

Abbreviations
2′3′-cGAMP, 2′3′-Cyclic guanosine monophosphate–adenosine monophosphate; cGAS, cyclic guanosine-adenosine synthetase; IFI16, interferon-gamma-inducible protein 16; IFN, interferon; IFN-β, interferon beta; IRF3, interferon regulatory factor 3; MPyV, mouse polyomavirus; MX-1, MX Dynamin Like GTPase 1; p204, protein 204; STING, the stimulator of IFN genes.

Two nonhuman members of the family, the simian virus 40 (SV40) and the mouse polyomavirus (MPyV), have served as models for the study of the polyomavirus replication cycle, cellular processes, such as DNA replication and endocytosis, targeting the cell nucleus, and mechanisms of cell transformation. In this study, MPyV was used as a model polyomavirus to study the host mechanisms of viral DNA sensing. MPyV has a capsid with icosahedral symmetry composed of 72 pentamers of the major capsid protein, VP1. One molecule of the two minor capsid proteins, either VP2 or VP3, is noncovalently bound to the central cavity of each VP1 pentamer [11,12]. Inside the capsid, the circular double-strand (ds) DNA genome, approximately 5.3 kbp long, forms a condensed nucleocore with cellular 2A, 2B, 3, and 4 histones. The genome encodes four early regulatory proteins, large tumor antigen (LT), small T antigen (ST), middle T (MT), and tiny T antigen (reviewed in [13]), and three late gene structural proteins, VP1, VP2, and VP3. The genomes of polyomaviruses are transcribed and replicated in the cell nucleus. Electron microscopy studies of MPyV minichromosomes isolated from cell nuclei have shown that there are gaps free of nucleosomes present in approximately 20% of genomes. The gaps were mapped to the regulatory region, between the origin of replication (ORI) and late transcription start [14–16].

MPyV virions are internalized by host cells in monopinocytic vesicles and sorted through the early and late endosomes to the endoplasmic reticulum (ER) [17–19]. In the ER, the virus undergoes conformational changes that promote the exit of remodeled and partially disassembled virions to the cytosol [20–22]. At approximately 6 h postinfection (hpi), the partially disassembled viral particles interact with importins, which promote viral DNA translocation to the nucleus via nucleopores [23]. Once the viral genomes appear in the nucleus, transcription of the early region starts. Genome replication initiated by the LT antigen and coincident late transcription from the complementary strand can be detected from 12 to 15 hpi. At 20–24 hpi, there is a dramatic change in the relative abundance of the late/early transcripts dependent on massive viral DNA replication (reviewed in [13]). The new virus progeny is assembled and released from infected cells at 40–48 hpi [24].

Innate immune DNA sensors are proteins that recognize pathogenic DNA and induce the production of interferon (IFN) and other host cytokines. DNA sensors are localized in the endosomes, free in the cytosol and, unexpectedly, in the cell nucleus. Toll-like receptor 9 (TLR9) is the only DNA sensor found in endosomes [25–27], whereas at least 11 DNA sensors were found to signal from the cytosol: DNA-dependent activator of IFN regulatory factors (DAI) [28]; RNA polymerase III (converting the cytosolic poly (dA-dT) DNA into 5′-pppRNA, which is then recognized by the RIG-I pathway) [29]; absence in melanoma 2 (AIMS 2) [30]; IFN-gamma-inducible protein 16 (IFI16) or its mouse ortholog, protein 204 (p204) [31–33]; leucine-rich repeat containing protein [34]; Ku70/Ku80 protein [35]; DEAH box polypeptide 9 and DHX36 (DEAH box polypeptide 36) [36]; DDX41 helicase [37]; cyclic guanosine-adenosine synthetase (cGAS) [38,39]; and IFN-inducible protein X (IFIX) [40]. Of these sensors, IFI16 (p204 in mice) and IFIX [32,40–43] were found to sense DNA in the nucleus. In addition, cGAS, described as a cytosolic sensor, is found in both the cytoplasm and the cell nucleus and there is one report suggesting its nuclear activation. The authors showed that in dendritic cells, the overproduction of cGAS fused to the nuclear localization signal (NLS) functionally upregulates the cellular innate immune responses [44]. The mechanisms used by DNA nuclear sensors to distinguish self-DNA from foreign DNA in the nucleus are an emerging topic of study [44–52]. It was shown that nucleosomes are barriers that prevent IFI16 from targeting self-DNA in the nucleus [45]. Likewise, it was shown that cGAS anchors nucleosomes. The nucleosome-binding interface was shown to be occupied by the DNA binding surface of the sensor, thus preventing sensing of self-DNA [53]. For IFI16 and cGAS, post-translational modifications including phosphorylation, acetylation, glutamylation, and ubiquitination have been shown to affect the activity or distribution of the protein [41,46–48,51,54,55].

At present, the most well-characterized mechanisms of DNA sensing are those mediated by IFI16 (p204 homolog) and by cGAS. The nuclear sensing of viral DNA by IFI16 has been studied widely in herpes viral infections. In detail, after the binding of IFI16 to herpesvirus genomes, IFI16 is acetylated and exported to the cytosol where it is available for interaction with the stimulator of IFN genes (STING) [56,57]. Further studies showed that IFI16 or p204 oligomerizes on DNA to induce the formation of filaments [45,50,58,59]. Coimmunoprecipitation experiments revealed that IFI16 forms complexes with STING and promotes the recruitment and activation of Tank-binding kinase 1 (TBK1). A model was proposed, in which IFI16 filaments recruit STING and TBK1, resulting in the phosphorylation of STING (at serine 366 in humans and 365 in mice). The phosphorylation of STING induces the recruitment of IFN-regulating

factor 3 (IRF3) and its phosphorylation via TBK1. The activation of IRF3 transcription factor results in IFN type I production [60,61].

The sensor cGAS binds to DNA in the cytoplasm and catalyzes the synthesis of cyclic guanosine-adenosine di-phosphate, 2′3′-Cyclic guanosine monophosphate–adenosine monophosphate (2′3′-cGAMP) [62]. The dinucleotide 2′3′-cGAMP binds to STING, which is then translocated to perinuclear areas where it interacts with TBK1 and the signaling proceeds as described for IFI16, resulting in the production of IFN type I.

We hypothesized that MPyV genomes could be sensed by DNA sensors either at early times postentry when the virus transported in endosomes is released into the cytosol to be imported to the nucleus or, alternatively, later after infection when the viral DNA replicates in the cell nucleus. In this study, we have shown that the MPyV virus is hidden from innate immune system recognition at early postinfection times. Nevertheless, viral DNA genomes are sensed during replication in the nucleus. MPyV genomes are sensed by p204 in the nucleus, while in the cytoplasm, viral DNA leaked from the nucleus and micronucleus-like bodies (which increase in incidence with the progress of infection) are sensed by cGAS.

Results

Interferon response is detected at late stages of the MPyV infection cycle

Interferon response to DNA occurs extremely rapidly. Previously, it has been described that mouse fibroblasts already produce an abundance of IFN beta (IFN-β) at 2 h after DNA transfection. In addition, murine skeletal myoblasts were also shown to produce IFN-β at 4 h after DNA transfection [63,64]. To study whether MPyV induced an IFN response in its natural host and to evaluate the possible time when the response was induced, we followed the expression of *IFN*-β and the IFN-regulated gene *MX-1* by qPCR in mouse fibroblasts (3T6 cells) within the time interval of 5–30 hpi. Representative experiments are displayed in the graphs in Fig. 1. Using five multiplicity of infection (MOI; Fig. 1A) and MOI 30 (Fig. 1B), we detected the upregulation of IFN-β mRNA in the cells from 24 hpi, with an increase at 30 hpi. In addition, significant upregulation of MX Dynamin Like GTPase 1 (MX-1) mRNA was detected at 30 hpi in both MOI 5- (Fig. 1A) and MOI 30-infected cells (Fig. 1B). Interestingly, at 30 hpi, the levels of IFN-β and MX-1 mRNA were higher in cells infected with a higher MOI (sevenfold for IFN-β and twofold for MX-1). Our data suggested that the main IFN response was launched at late postinfection times when viral DNA replication occurs and that the strength of the IFN response was dependent on MOI.

We noticed that the strength of IFN response induced by MPyV, in cells infected with MPyV MOI 30, was low when compared with responses obtained previously in mouse fibroblasts transfected with plasmid DNA (pDNA) [63]. To verify this, we exposed 3T6 cells to different stimuli, such as pDNA, CpG, dinucleotides, polyinosinic:polycytidylic acid (poly (I:C)), or 2′3′-cGAMP (Fig. 1C,D), for the indicated times (described in Materials and methods), and we measured the expression of *IFN*-β and *MX-1* genes by qPCR. The results are presented in Fig. 1C,D. We observed that 3T6 fibroblasts stimulated with pDNA or other stimuli upregulated the IFN-β mRNA by 4000- to 80 000-fold. In contrast, for MPyV infection at MOI 30 (Fig. 1B), IFN-β mRNA was upregulated only by approximately 300-fold. The levels of MX-1 mRNA differed based on the stimulus applied, but were, in some cases, comparable with those induced by MPyV. The data suggested that the induction of *IFN*-β gene expression in response to MPyV infection was moderate in comparison with the responses induced by pDNA or other stimuli, whereas the regulation of the IFN-inducible *MX*-1 gene appears to be tightly controlled in 3T6 cells.

Interferon response to MPyV infection is dependent on the activation of STING and IRF3 proteins

Next, we focused on signaling related to the IFN response. We followed the time of activation (by phosphorylation) of IRF3, an essential transcription factor for *IFN*-β gene regulation. In addition, we also followed the phosphorylation of STING, a protein described as mediator of the IFN type I production in response to pathogenic intracellular DNA and a variety of intracellular pathogens. By western blotting, we detected the phosphorylation of both STING and IRF3 at 24 hpi (Fig. 2A). At 18 hpi, we did not detect phospho-STING or phospho-IRF3; thus, we concluded that activation occurred within 18–24 hpi. Accordingly, confocal microscopy images of the cell sections revealed phosphorylated STING (green) as patches in the cytoplasm of cells at 24 hpi, but not in the control (mock-infected) cells (Fig. 2B). These results suggested that MPyV is recognized by the immune system late postinfection and that the viral nucleic acids were likely to be first sensed in the nucleus during viral DNA replication.

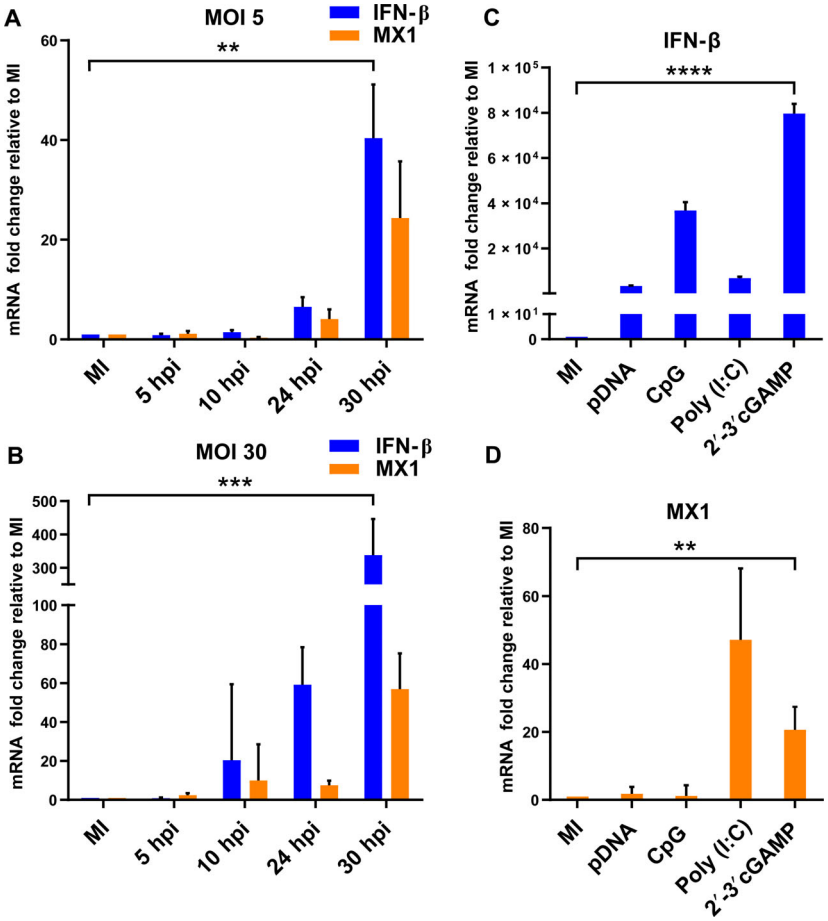

Fig. 1. Kinetics of the IFN response during MPyV infection. (A, B) Mouse 3T6 fibroblasts were infected with MPyV at 5 MOI (A) or 30 MOI (B). After 5, 10, 24, and 30 hpi, the cells were collected, and RNA was isolated. (C, D) 3T6 cells were stimulated with pDNA, CpG, poly (I:C), or 2′3′-cGAMP and collected at the indicated times (described in Materials and methods) for RNA isolation. For all samples (A–D), the levels of IFN-β and MX-1 RNAs were detected by qPCR and normalized to the GAPDH mRNA levels. The displayed data correspond to one representative experiment from at least three independent repeats (each experiment was performed with a different viral stock), and the presented values correspond to the mean of biological triplicate ± SD. Selected data were compared using Student's *t*-test. Asterisks indicate *P*-values representing statistically significant differences. For (A) IFN-β, $^{**}P = 0.0024$; for (B) IFN-β, $^{***}P = 0.0007$; for (C) IFN-β, $^{****}P = 0.0001$ and (D) MX-1, $^{**}P = 0.0074$. For the experiments, mock-infected cells (MI) were used as the control.

To determine the influence of STING on the signaling leading to IFN-β production during MPyV infection, we used a MEF-STING knockout (MEF-STING KO) and parental MEF-STING wild-type (wt) cell lines. We first confirmed the absence of STING protein in the KO cells by immunoblotting (Fig. 2C, upper western blot). Next, we analyzed IRF3 activation in response to MPyV in the KO cells. The phosphorylated IRF3 isoform was not detected in the infected MEF-STING KO cells, but was abundant in the infected MEF-STING wt cells (Fig. 2C, lower western blot). We then followed the IFN response by qPCR (Fig. 2D) and found that there was no upregulation of *IFN-β* or *MX-1* gene expression in the MEF-STING KO cells (Fig. 2D). In contrast, the MEF-STING wt cells responded to MPyV infection by increasing levels of INF-β (188-fold) and MX-1 (48-fold) mRNAs. To characterize the ability of MEF-STING KO cells to respond to other stimuli, such as RNA, the cells were treated with poly (I:C). We followed the levels of phosphorylated IRF3 by western blotting (Fig. 2E) and IFN mRNA levels by qPCR (Fig. 2F). We found that MEF-STING KO cells could activate IRF3 and induce *IFN-β* and *MX-1* gene expression when stimulated by RNA. Thus, our results showed that STING protein is essential for the induction of the IFN-β response during MPyV infection. Given that STING and IRF3 are phosphorylated in the same time frame during MPyV infection (Fig. 2A) and that STING KO cells do not activate IRF3 in response to MPyV infection (Fig. 2C), this provides support for the model in which activated STING promotes the recruitment of IRF3 to TBK1 active sites [61].

The presence of MPyV genomes in the cell nucleus is crucial for the induction of the interferon response

To further confirm the essential role of late (nuclear) phases of MPyV infection in the DNA sensing in contrast to the early phase, when the virus travels undetected by sensors in endosomes (Fig. 1), we used a mutated MPyV that was unable to translocate efficiently to the cell nucleus (a mutant previously constructed and

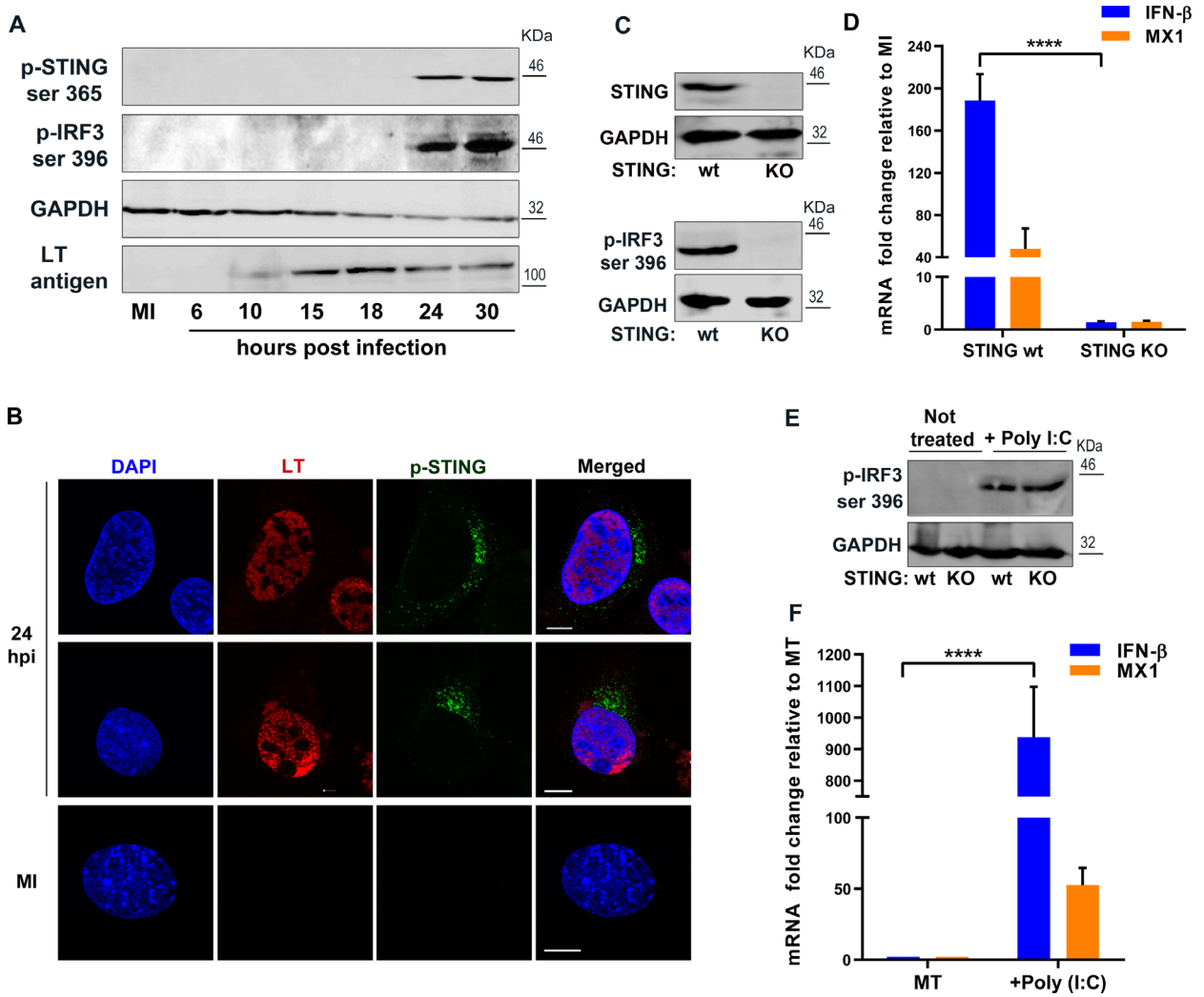

Fig. 2. STING and IRF3 are involved in the IFN response induced by MPyV. (A) Mouse 3T6 fibroblasts were infected with MPyV (MOI = 10). At the indicated times, cell lysates were prepared and phospho-IRF3 (p-IRF3), phospho-STING (p-STING), or GAPDH and LT antigen as controls, were detected by western blotting. (B) Mouse 3T6 fibroblasts were either mock-infected (MI) or infected with MPyV (MOI = 3), fixed at 24 hpi, and stained by DAPI (blue) and by antibodies directed to MPyV early LT antigen (red) and phospho-STING (p-STING; green). Confocal microscopy images of representative cell sections are presented. Bars = 10 μm. (C) MEF-STING KO or STING wt cells were infected with MPyV (MOI = 20) and the cell lysates were prepared at 30 hpi. The samples were analyzed by western blotting for the presence of STING, phospho-IRF3 (p-IRF3), and GAPDH as a loading control. (D) MEF-STING KO and STING wt cells were mock-infected or infected with MPyV (MOI = 20). At 30 hpi, RNA was isolated and subjected to qPCR for quantification of IFN-β, MX-1and GAPDH mRNAs, with values normalized to the transcripts in the mock-infected cells (MI). (E, F) MEF-STING KO or STING wt cells were treated with poly (I:C) (+) or not treated (MT) and cells were collected after 16 h. Cell lysates were prepared and the presence of phospho-IRF3 (p-IFR3) and GAPDH (as a loading control) was followed by western blotting (E). RNA was isolated and the IFN-β, MX-1, and GAPDH mRNA levels were quantified by qPCR (F). For (A), (C), and (E), each of the presented western blots is representative of at least two independent experiments. For (D) and (F), the presented data correspond to the mean values of three independent experiments; the corresponding SD values are presented. Selected data were compared using Student's *t*-test. Asterisks indicate *P*-values representing statistically significant differences. For (D) IFN-β, ****$P = 0.0001$ for (F) IFN-β, ****$P = 0.0001$.

characterized in our laboratory) [23]. The virus mutant that lacks the NLS of the structural proteins enters cells efficiently and can be released, similar to the wt virus, into the cytosol after its trafficking to ER. However, because of the lack of NLS, the virus exhibits defective nuclear entry via nucleopores and its infectivity is decreased by 80%. Here, stocks of the mutated virus were produced after transfection of the mutated

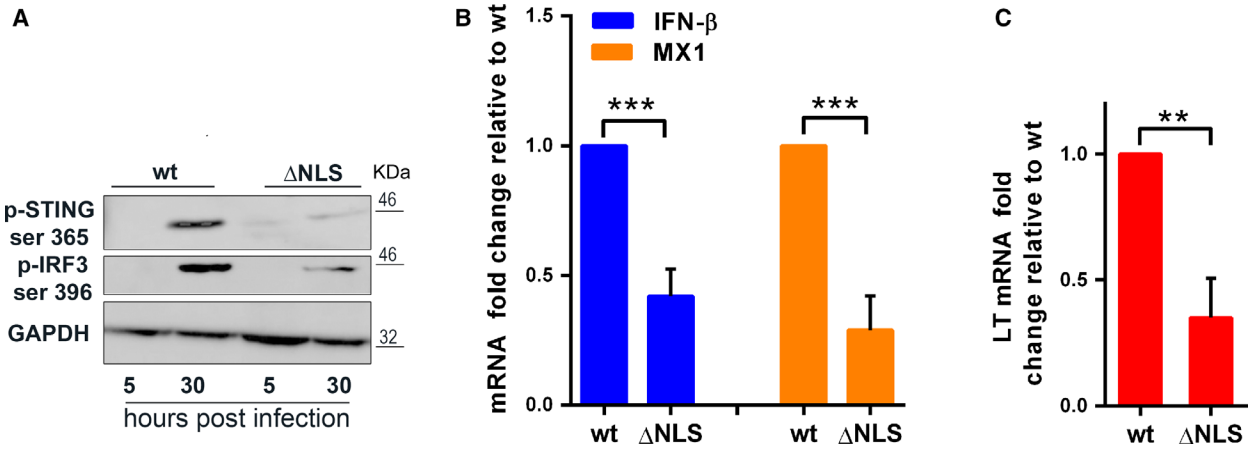

Fig. 3. IFN response in MPyV-infected cells is strongly dependent on the presence of viral genomes in the cell nucleus. 3T6 fibroblasts were infected with MPyV-wt (wt) or MPyV-mutated in NLS (Δ NLS) with MOI corresponding to 200 genomes per cell, as quantified by qPCR. The cells were collected at 5 or 30 hpi for the preparation of cell lysates and 30 hpi for isolation of RNA. (A) Cell lysates were subjected to western blotting and assayed for phospho-IRF3 (p-IRF3), phospho-STING (p-STING), and GAPDH. The western blot shown is representative of two experiments. (B) RNAs were isolated and the mRNA for IFN-β, MX-1 (B), or for LT (C) were measured by qPCR. For (B) and (C), the presented data correspond to mean values of three independent experiments (performed with three different viral stocks); the corresponding SD values are presented. For each experiment, the values were normalized to those of wt virus. The data were compared using Student's *t*-test. Asterisks indicate *P*-values representing statistically significant differences (IFN-β, ***$P = 0.0006$; MX-1, ***$P = 0.0007$; LT, **$P = 0.0021$).

genomes. In the same way, wt MPyV was prepared as a control. We followed the IFN response (as described previously) and the levels of infection by measuring LT viral antigen production. The western blot (Fig. 3A) revealed that IRF3 and STING phosphorylated proteins were markedly lower in the cells infected with NLS mutant virus compared with that in wt MPyV-infected cells. In agreement, we found the expression of the IFN-related genes significantly decreased in the cells infected with the NLS mutant virus. Specifically, the levels of IFN-β mRNA decreased by 60% and the levels of MX-1 mRNA decreased by 70% (Fig. 3B). Accordingly, lower expression of LT antigen (by 70%) was observed in the cells infected with the NLS mutant virus compared with that of cells infected with the wt virus (Fig. 3C). These results strongly support the above observation that IFN induction is associated with the late phase of infection, in which viral genomes replicate in the cell nucleus.

The DNA sensor p204 is involved in *IFN*-β induction during MPyV infection

Previously, human herpesvirus was shown to be sensed in the nucleus by the innate immune DNA sensor, IFI16. We hypothesized that the mouse protein related to IFI16 protein, p204, could sense MPyV DNA in the nucleus during viral genome replication. To test the involvement of p204 in the induction of IFN by MPyV, we followed the IFN response in cells with downregulated p204. For this, we used small interfering RNAs (siRNAs) against p204 (si-p204) or random siRNA as the control. Knockdown efficiency was confirmed by western blotting (Fig. 4A). The levels of p204 decreased approximately by 60% in the cells treated with si-p204 in comparison with those in untreated cells or cells treated with random siRNA. The effect of p204 knockdown on *IFN*-β and *MX-1* transcription was assessed by RT-qPCR. The results (Fig. 4B) showed that both IFN-β and MX-1 mRNA levels were significantly reduced (by 65% and 55%, respectively) in the p204-knockdown cells compared with the nonsilenced control cells. Finally, a substantial decrease (by 47%) of activated IRF3 in p204-knockdown cells was estimated from phospho-IRF3 and GAPDH band densities on the western blot (Fig. 4C). To better understand the mechanism of p204 activation, we assessed the localization of p204 and replicating MPyV genomes in infected cells by confocal microscopy. For that, we labeled MPyV genomes by fluorescence *in situ* hybridization (FISH), p204 by a specific antibody, and whole DNA by 4′,6′-diamidino-2-phenylindole (DAPI). Using a standard fixation protocol, p204 was spread throughout the nucleus and clear colocalization with MPyV genomes was observed only sporadically (data not shown). To uncover interaction between viral

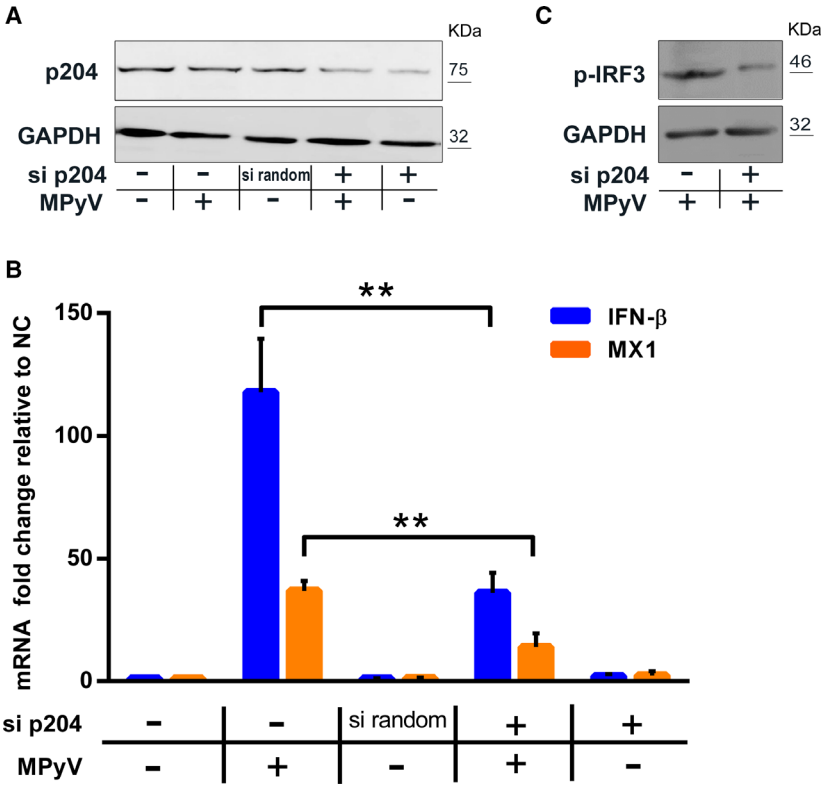

Fig. 4. p204 plays a role in IFN induction by MPyV infection. (A–C) Mouse 3T6 fibroblast cells were transfected with p204 siRNA. Random siRNA transfection or untransfected cells were used as the control. After 48 h, the cells were infected with MOI = 20 or mock-infected and incubated for 30 h. (A) A representative western blot (of the three prepared) is presented. (B) IFN-β or MX-1 mRNA levels were measured by qPCR. The values were normalized to GAPDH mRNA levels. The data presented correspond to mean values of three independent experiments; the corresponding SD values are presented. Samples were compared by Student's *t*-test. Asterisks indicate *P*-values representing statistically significant differences (IFN-β, $^{**}P = 0.0053$; MX1, $^{**}P = 0.0064$). (C) Cell lysates were prepared and subjected to immunoblotting for evaluation of the levels of phospho-IRF3 (p-IRF3) and GAPDH. A representative western blot (of the three prepared) is presented.

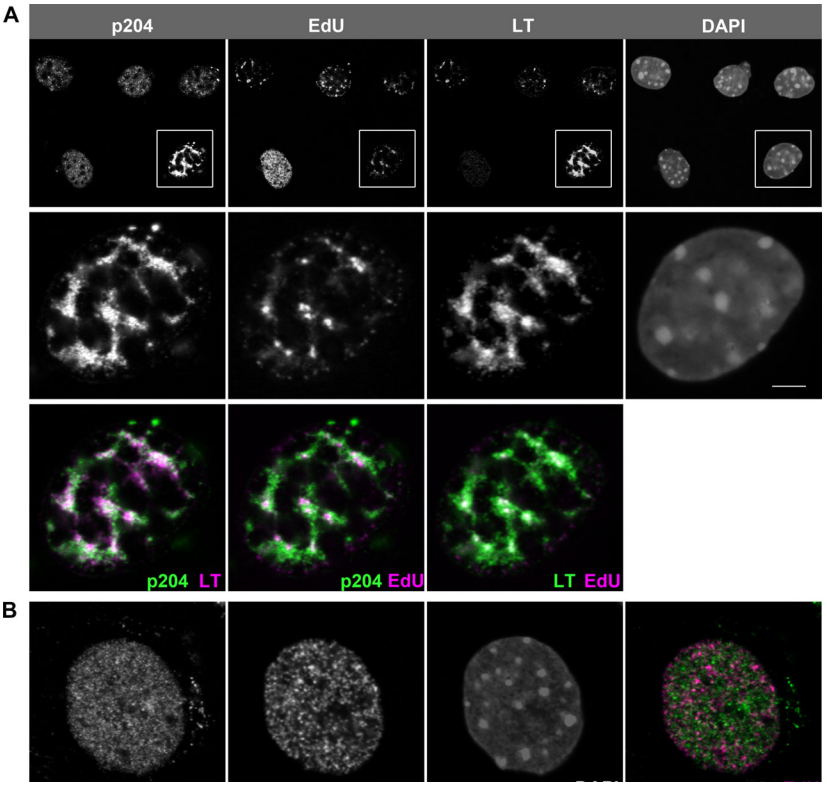

Fig. 5. p204 accumulates in areas of MPyV DNA replication. MEF cells were infected with MPyV (MOI = 5) (A) or mock-infected (B) and incubated for 24 h. EdU was added for the last 30 min of incubation. Then, cells were treated for 5 min with pre-extraction buffer and fixed. For immunofluorescence, cells were stained with anti-p204 (green) and anti-MPyV LT (far red, displayed as magenta or green) antibodies. EdU was visualized by the Click-iT EdU reaction (red, displayed as magenta) and DNA was stained by DAPI (displayed as white). Representative confocal cell sections were analyzed. Scale bar = 5 μm.

DNA and p204, the cells were stained using a protocol including prefixation permeabilization (using a pre-extraction buffer) [65]. Replicating genomes were labeled by EdU and the p204 protein and viral LT antigen were detected by using specific antibodies. We found that p204 accumulated in the areas of replication/transcription of viral genomes where it markedly colocalized with EdU-labeled replicating viral genomes and

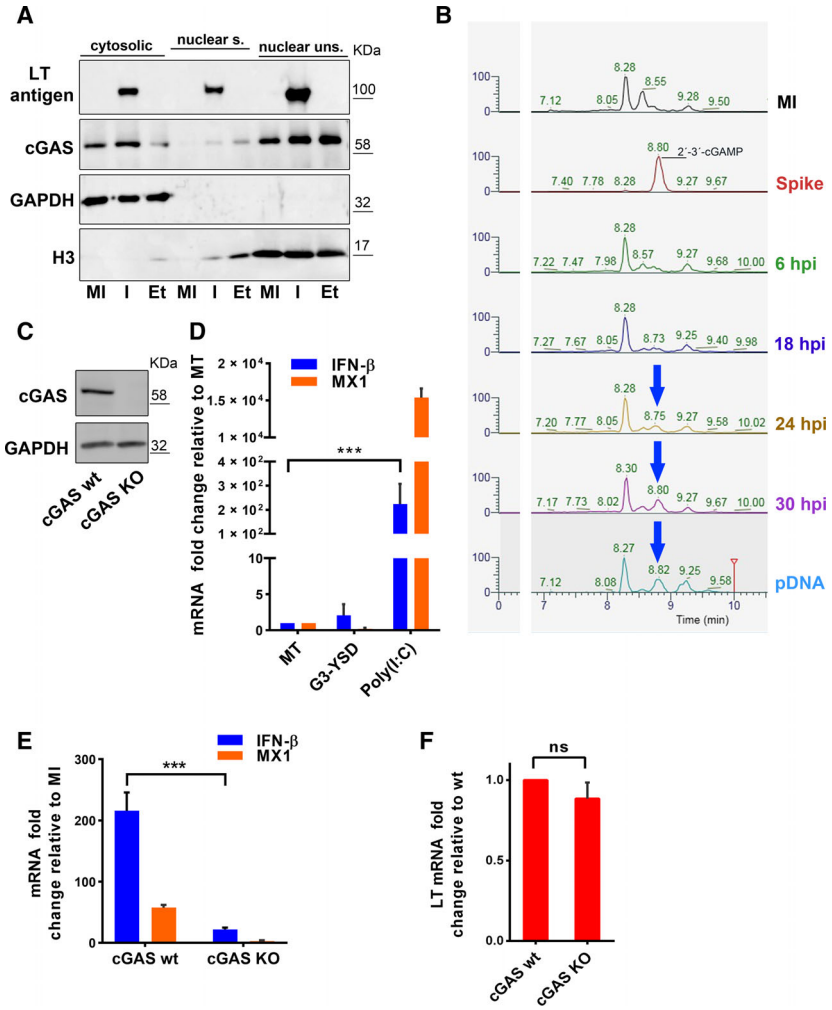

Fig. 6. cGAS is activated during MPyV infection. (A) Mouse 3T6 fibroblasts were mock-infected (MI) or infected (I) with MPyV (MOI = 3) for 24 h or treated with etoposide (Et) for 6 h. Then, the cells were collected and subjected to subcellular fractionation. The fractions [cytosolic and nuclear-soluble (s), and nuclear-insoluble (ins)] were immunoblotted and stained with antibodies against cGAS or, as controls, against GAPDH, Histone 3 (H3), or LT. (B) Mouse 3T6 fibroblasts were infected with MPyV (MOI = 5), and at the indicated times, dinucleotides were extracted from the cells, and samples were analyzed by LC-MS for detection of 2′3′-cGAMP. Mock-infected cells or cells transfected were included as controls. In addition, an internal control of commercial 2′3′-cGAMP was spiked into the lysate of mock-infected cells. Specific transitions for 2′3′-cGAMP (675.1 > 136.1, 675.1 > 524.1, 675.1 > 312.1, 675.1 > 506.0, 675.1 > 152.1, 675.1 > 476.0, 675.1 > 330.0) were used to detect 2′3′-cGAMP. In the graph, transition 506.0 is shown. 2′3′-cGAMP (retention time: 8.75–8.82 min) is shown in the spike and indicated by arrows in the samples when present. (C) MEF-cGAS KO or wt MEF were cultivated for 24 h, and the cell lysates were prepared and subjected to western blotting for detection of cGAS. GADPH was detected as the control. (D) MEF-cGAS KO cells were either mock-transfected (MT) or transfected with 26-mer DNA (G3-YSD) or with poly (I:C). After 16 h, the cells were collected, and RNA was isolated. IFN-β, MX-1, and GAPDH mRNA levels were quantified by qPCR. (E, F) MEF-cGAS KO and cGAS wt cells were infected with MPyV (MOI = 5) and incubated for 30 h before collection for RNA preparation. RNAs were isolated and used to measure IFN-β, MX-1 (E), and LT (F) mRNA levels by qPCR. (D–F) The data presented correspond to mean values of three independent experiments; the corresponding SD values are presented. Selected data were compared using Student's *t*-test. Asterisks indicate *P*-values representing statistically significant differences. For (D) IFN-β, ***$P = 0.0004$; for (E) IFN-β, ***$P = 0.0002$; for (F) the *P*-value obtained did not show statistically significant differences, denoted as ns, $P = 0.0807$.

LT antigen (Fig. 5A). In mock-infected cells (Fig. 5B), p204 was distributed throughout the nucleus in distinct dots that, in part, overlapped with EdU-labeled replicating cellular DNA (Fig. 5B). Collectively, our results showed that p204 was involved in the induction of IFN response by MPyV and indicated that p204 became activated in the cell nucleus. However, to uncover the detailed role of p204, further research is required.

The DNA sensor cGAS is essential for IFN-β production in MPyV-infected cells

Although described as a cytosolic sensor, cGAS is located not only in the cytoplasm but also in the cell nucleus. During DNA transfection, both IFI16 and cGAS sense DNA independently. In contrast, during herpesvirus infection, cGAS was found to bind to IFI16, promoting its stability by preventing its degradation [57]. Therefore, we assessed whether cGAS participated in the IFN response induced by MPyV.

First, we followed the subcellular localization of cGAS in infected cells by cell fractionation. As controls, we also fractionated noninfected cells and noninfected cells treated with etoposide. Etoposide, upon forming a ternary complex with DNA and topoisomerase II, causes breaks in dsDNA. It has been shown that upon DNA damage, cytosolic cGAS translocates to the nucleus [46]. The cells were fractionated into three fractions: cytosolic, nuclear-soluble, and nuclear-insoluble, and we detected cGAS by western blotting (Fig. 6A). We found that during infection, as well as in uninfected cells, cGAS was found in both the nuclear-insoluble fraction and the cytosolic fraction. In contrast with cells treated with etoposide, we did not observe significant mobilization of the cytoplasmic cGAS pool to the nucleus.

As the activation of cGAS in response to DNA binding results in the production of 2′3′-cGAMP, we followed the production of the dinucleotide during infection by liquid chromatography-mass spectrometry (LC-MS). Infected or mock-infected 3T6 cells were harvested from 6 to 30 hpi and processed for the detection of 2′3′-cGAMP. We first detected 2′3′-cGAMP at 24 hpi and its synthesis has increased substantially by 30 hpi (Fig. 6B).

To determine whether cGAS activation had any effect on the induction of IFN expression by MPyV, we analyzed IFN responses in MEF-cGAS KO or MEF-cGAS wt cells. First, we verified the knockout of cGAS by western blotting (Fig. 6C). Next, we performed an additional control, to confirm that the cGAS KO cells responded to RNA but did not respond to DNA stimulus via cGAS. To achieve this, we transfected the cells with either poly (I:C) or with the cGAS agonist G3-YSD. G3-YSD is a 26-mer DNA sequence derived from the HIV-1 RNA genome, which has a Y-shape owing to a palindromic sequence flanked by unpaired guanosine trimers. This DNA sequence has been identified as a minimal recognition motif required for cGAS activation. After measurement of the mRNA levels by qPCR, we found that in the MEF-cGAS KO cells, poly (I:C) induced the upregulation of *IFN-β* and *MX-1* whereas G3-YSD did not induce an IFN response (Fig. 6D). Next, we used qPCR to measure the levels of IFN-β and MX-1 mRNA in MPyV-infected MEF-cGAS KO or MEF-cGAS wt cells (Fig. 6E,F). In cGAS KO cells, the IFN-β mRNA levels were dramatically lower (by ninefold) than in MEF-cGAS wt cells. Accordingly, while high production of MX-1 mRNA was induced in MEF-cGAS wt cells, almost no detectable mRNA production was observed at the same time postinfection in cGAS KO cells. As an infection control sample, we measured the levels of mRNA of LT antigen in the MEF-cGAS KO and MEF-cGAS wt cells and found no significant difference. Our results showed that there was a particularly important contribution from cGAS activation in the IFN response induced by MPyV. Nevertheless, it is important to highlight that the IFN response is not completely abolished by the absence of cGAS. Thus, we can conclude that at least two mechanisms are activated in parallel during MPyV infection: viral genome sensing by p204 and activation of cGAS.

cGAS senses DNA leaked from the nucleus to cytoplasm and micronucleus-like bodies

Further, we addressed the question of whether cGAS participated in IFN induction by MPyV through sensing of viral DNA in the nucleus, as recently described [44], or if there are other mechanisms that lead to cGAS activation. Using confocal microscopy, we followed whether cGAS present in the nucleus had an affinity for replicating MPyV genomes. To achieve this, mouse fibroblasts expressing cGAS-EGFP were prepared and infected with MPyV. Then, cells were subjected to FISH using sequences of the MPyV genome as a probe (Fig. 7). Surprisingly, we found colocalization of viral DNA with cGAS in different subcellular compartments. We observed strong colocalization of cGAS with viral DNA probably leaked from the nucleus to the cytosol in a subpopulation of cells (Fig. 7A–C). Further, in a subpopulation of cells, the cGAS signal overlapped with MPyV genomes in the

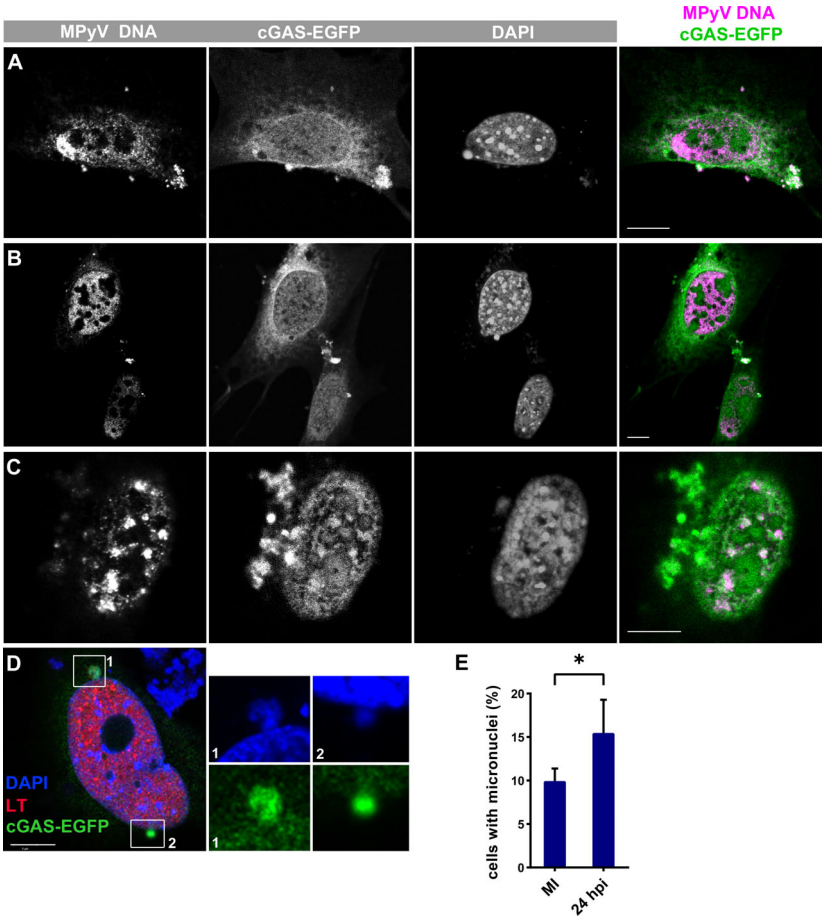

Fig. 7. cGAS colocalizes with MPyV genomes and micronucleus-like bodies. (A–D) 3T6 cells expressing GFP-cGAS were infected with MPyV (MOI = 3) and fixed at 24 hpi. (A–C) Cells were stained with antiGFP (green) to enhance the signal, and then subjected to FISH with MPyV DNA probe labeled with biotin, followed by staining with anti-biotin antibody (magenta). Confocal sections of the cells displaying colocalization of GFP-cGAS with MPyV genomes are presented. Bars = 10 μm. (D) Cells were stained with anti-LT antibody (red), cGAS-EGFP was visualized by anti-GFP (green), and DNA was labeled by DAPI staining. Confocal sections of the cells displaying micronucleus-like structures colocalizing with GFP-cGAS are presented. Bars = 10 μm. (E) Mouse fibroblasts infected at MOI 3 or mock-infected were fixed at 24 hpi and DNA was labeled by DAPI staining. The cells were scored for the presence of micronucleus-like bodies; the results are summarized in the graph. The data presented correspond to mean values of three independent experiments (At least 250 cells in each experiment were examined); the corresponding SD values are presented. Student's *t*-test was performed. Asterisks indicate *P*-values representing statistically significant differences (**P* = 0.0152).

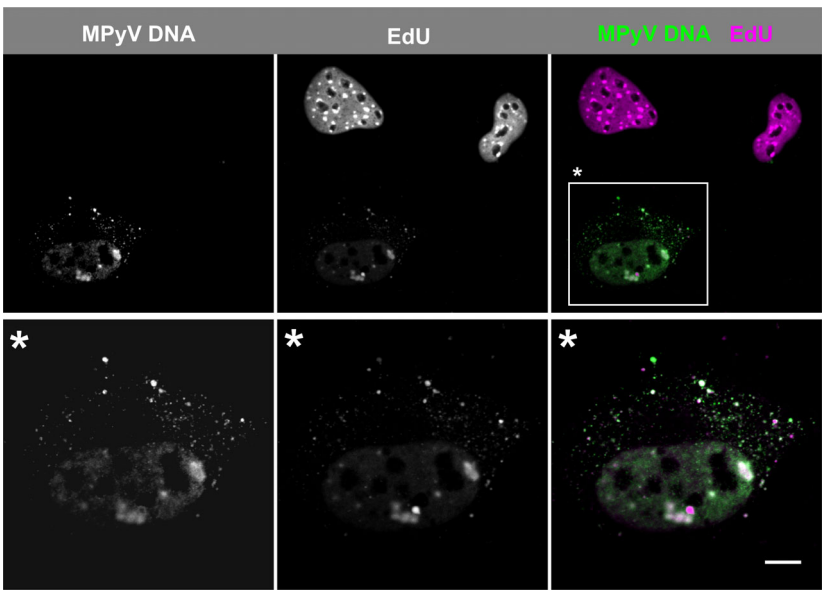

Fig. 8. Leakage of DNA to cytosol during MPyV infection. MEF cells were infected with MPyV (MOI = 3) in presence of EdU. After 24 h, the cells were fixed, the Click-iT EdU reaction was performed, and the cells were used for FISH with MPyV DNA probe labeled with biotin and detected with anti-biotin antibody. Representative confocal section of cells displaying EdU DNA (magenta) and viral DNA (green). A white asterisk is used to highlight the infected cell among the uninfected ones. Bar = 5 μm.

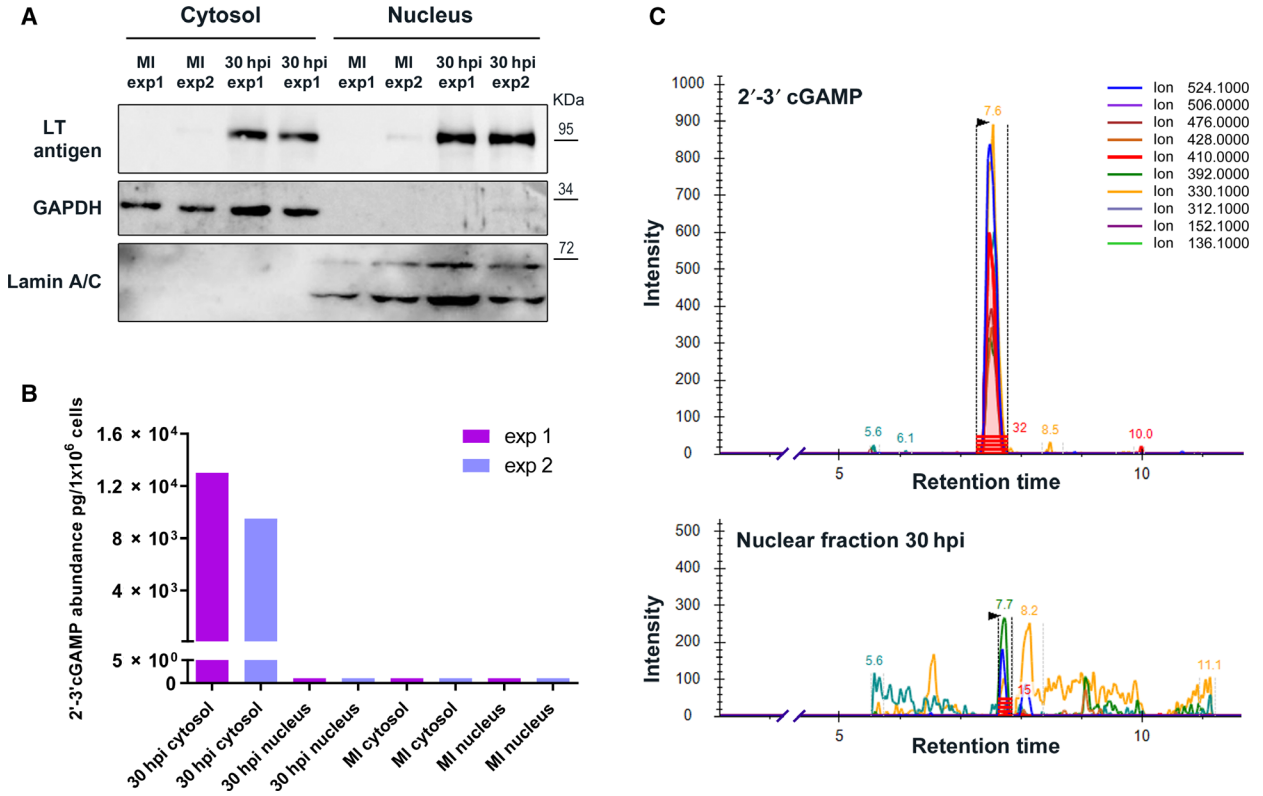

Fig. 9. 2′3′-cGAMP is detected only in the cytosolic fraction of infected cells. Mouse fibroblasts were infected with MPyV at MOI 5 or mock-infected (MI). After 30 h, the cells were fractionated. Two independent experiments were performed (A) The fractions were verified by western blotting using antibodies against lamin A/C for the nuclear fractions, GAPDH for the cytosolic fraction, and LT (to verify infectivity). One of two representative experiments is displayed. (B) The cell fractions were used for detection of 2′3′-cGAMP by competitive ELISA. Standards were prepared in the cell lysis buffers. Two independent experiments are displayed (exp1 and exp2). (C) Nuclear fractions were analyzed by LC-MS. Specific transitions for 2′3′-cGAMP (675.1 > 136.1, 675.1 > 524.1, 675.1 > 312.1, 675.1 > 506.0, 675.1 > 152.1, 675.1 > 476.0, 675.1 > 330.0) were used to detect 2′3′-Cgamp. One of two representative experiments is displayed. As the spike, commercial 2′3′-cGAMP was used.

nucleus (Fig. 7C) and, unexpectedly, we also found micronucleus-like bodies loaded with cGAS (Fig. 7D).

Next, we compared the number of micronucleus-like bodies in mock-infected and infected cells at the time postinfection when IFN induction became detectable. For this experiment, we used cells not overexpressing cGAS to exclude any effect of the overexpression on the formation of micronucleus-like bodies. MPyV-infected or mock-infected cells were fixed and subjected to DAPI staining; then, using confocal microscopy, micronucleus-like bodies were counted. Although we observed micronucleus-like bodies in both infected and mock-infected cells, the total number of micronucleus-like bodies in infected cells was significantly higher than in mock-infected cells (Fig. 7E).

To provide a more convincing demonstration that the viral cytosolic DNA detected in infected cells was leaked from the nucleus, we labeled the host and viral replicating DNA with EdU and then performed FISH for detection of MPyV genomes to search for overlapping signals in the cytosol. In detail, EdU was added to the growth medium at the beginning of infection and at 24 hpi click chemistry was used to detect EdU and FISH. As expected, we detected EdU and the MPyV genome signal colocalizing in the cytosol. In addition, only the EdU signal (not colocalized with MPyV genomes) apparently corresponding to leaked host DNA was detected in the cytosol (Fig. 8). Next, to determine whether the interactions of cGAS with MPyV minichromosomes in the cell nucleus resulted in cGAS activation, we analyzed the levels of 2′3′-cGAMP in separated cytosolic and nuclear fractions of infected cells. The separation of nuclear and cytosolic fractions was verified by western blotting (Fig. 9A) and the fractions were examined for 2′3′-cGAMP by competitive ELISA (Fig. 9B). We found an abundance

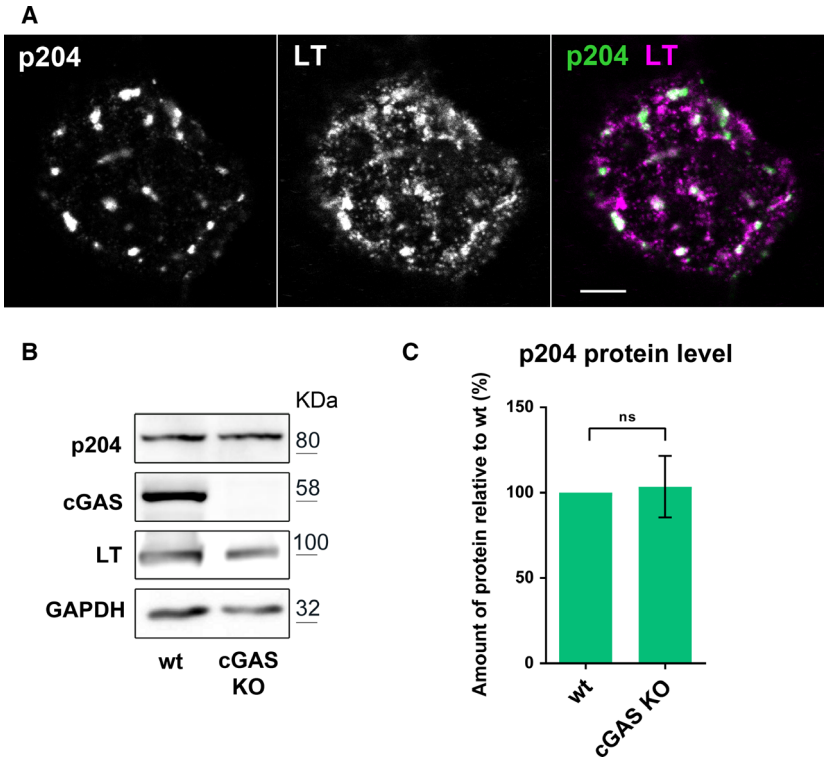

Fig. 10. Absence of cGAS did not affect either the interaction of p204 with the MPyV genomes or its level in cells. (A) MEF-cGAS KO cells were infected with MPyV (MOI = 3) and incubated for 24 h. The cells were treated for 5 min with pre-extraction buffer and then fixed. Next, the cells were stained with anti-MPyV LT antigen (magenta) and anti-p204 (green) antibodies. The image shows a confocal section of the nucleus of the infected cell. Scale bar = 5 μm. (B, C) MEF wt and cGAS KO cells were infected with MPyV (MOI = 5). At 30 hpi, cell lysates were prepared and analyzed by western blotting to follow the p204 levels. As a control, antibodies against cGAS, GAPDH, and LT antigen were used. Three independent experiments were performed (B). The graph represents comparison of levels of p204 (related to levels of GAPDH loading controls) in MEF-cGAS wt and MEF-cGAS KO cell lysates. The data presented correspond to mean values of three independent experiments; the corresponding SD values are presented. Student's *t*-test was performed. The *P*-value obtained did not show statistically significant differences, denoted as ns, $P = 0.85$ (C).

of 2′3′-cGAMP in the cytosolic fraction of infected cells. However, we did not detect any 2′3′-cGAMP in the nuclear fractions of infected cells, similar to all fractions of control (uninfected) cells. To confirm the absence of 2′3′-cGAMP in the nuclear fractions of infected cells by a second method, we analyzed the samples by LC-MS. A representative chromatogram of the nuclear fraction of infected cells is shown in Fig. 9C: 2′3′-cGAMP was not detected in the nuclear fractions; only traces of a dinucleotide with different spectra were found.

Our results strongly suggest that cGAS senses viral DNA present in the cytosol but is not activated in the nucleus of MPyV-infected cells. Colocalization of cGAS with viral genomes in the nucleus may represent an additional role of the nuclear cGAS independent of its activation. However, the activation of cGAS in the cytosol reflects its interactions not only with viral or cellular DNA leaked from the nucleus, but also with micronucleus-like bodies formed by genotoxic stress induced by the infection.

Absence of cGAS does not affect the interaction of p204 with MPyV genomes in the cell nucleus or the levels of p204

As the ability of cGAS to degrade IFI16 on the genomes of herpesviruses in the nucleus has been reported [57], we investigated whether cGAS had similar effects on p204 in MPyV infection. First, we assessed whether cGAS absence affects the colocalization of p204 with viral genome replication sites. To achieve this, we used confocal microscopy to examine the colocalization of p204 with LT viral antigen in cGAS KO cells (Fig. 10A). We found that p204 protein could be preferentially seen in LT spots, similar to infected wt cells (Fig. 5A). Thus, our results indicated that the absence of cGAS did not impair p204 localization on viral

DNA replication areas. In addition, we examined the possible contribution of cGAS to the prevention of fast turnover of p204. Therefore, we examined the levels of p204 protein in MPyV-infected cGAS KO and wt cells by western blotting. We found that at 30 hpi, the levels of p204 in lysates of both cell lines were comparable, regardless of the presence or absence of cGAS (Fig. 10B,C). The above results showed that cGAS did not stabilize p204 on viral genomes and suggested that the sensing of MPyV genomes by both DNA sensors occurs simultaneously, but independently.

Discussion

Nucleic acids of pathogens can be recognized through pattern recognition receptors by host cells. This leads to production of IFN and other hundreds of proteins with antiviral effects. In the past decade, many sensors of invading nucleic acids have been described and an understanding of the molecular bases of DNA and RNA immune recognition has emerged. Genomes of herpes simplex virus-1, kaposi's sarcoma-associated herpesvirus, vaccinia virus, murine gamma herpesvirus 68, adenovirus, hepatitis B virus, and HIV (reviewed in [66]) have been shown to be recognized by specific nucleic acid sensors. We therefore aimed to determine whether small DNA viruses, such as polyomaviruses, which travel to the nucleus in endosomal compartments and have genomes organized into minichromosomes, are recognized by host DNA sensors. We focused on the possible interactions between MPyV genomes and host DNA sensors, p204 (closely related to human IFI16) and cGAS. We found that regardless of the MOI, a moderate IFN response was launched not sooner than the late phase of infection (approximately 24 h), at the time when genome replication occurs.

The absence of IFN induction at early times postinfection suggests that the virus is hidden or invisible for the immune system when sorted through the endosomal system to ER. Although virions, partially disassembled in the ER, appear in the cytosol prior to their importin-mediated transfer to the nucleus [23], their genomes remain inaccessible to interaction with cytosolic DNA sensors for several reasons. At first, genomic DNA in polyomavirus virions is tightly packed in the form of a nucleocore condensed with cellular histones (except H1) and the capsid protein VP1, making it inaccessible to other protein interactions. Indeed, studies of polyomavirus have suggested that the release of the nucleocore into relaxed minichromosomes with nucleosomes occurs in the cell nucleus [67]. Subsequently, depending on cell type, only small fractions of internalized virions travel by productive endocytic pathway to the ER and then are released into the cytosol [19,23]. Substantial portions of virions remain in late recycling endosomes from where they exit cells and in endolysosomal compartments where they are subject to degradation. Moreover, in the cytosol, viruses can be degraded by proteosomes and any DNA released from proteasomes is probably degraded rapidly by exonuclease TREX-1 (which can degrade dsDNA). The activation of proteasomal systems during BK polyomavirus infection has been documented [68] and genomes of herpesvirus present in the cytosol or HIV reverse transcripts were degraded by TREX-1 [69,70]. All these previous observations account for the absence of IFN induction during transport of the virus into the nucleus and are in agreement with observed poor IFN response induced by the mutant virus with impaired ability to enter the nucleus (Fig. 3).

In the late phase of MPyV infection, replicating and transcribing viral DNA accumulate in the cell nucleus. The induction of IFN response at this time suggested the involvement of a nuclear DNA sensors. Therefore, we focused on the p204 protein—the mouse homolog of the human IFI16 protein found to sense herpesvirus DNA genomes in the cell nucleus. The ability to sense pathogenic DNA in the nucleus raised questions about the mechanisms preventing self-DNA recognition. IFI16 was found to be excluded from self-DNA recognition by the presence of nucleosomes that impede the one-dimensional movement (scanning) of the protein along DNA. The scanning of DNA allows the clustering of IFI16 required for its activation [45,50,58,59]. Herpesvirus genomes are chromatinized after they enter the nucleus. In addition, the density of nucleosomes is lower, their distribution more irregular, and histone association looser than that of the host DNA [71,72]. Therefore, their genomes are easily sensed by IFI16 in the nucleus [42]. Much smaller polyomavirus genomes are in complex with cellular histones already in virions, and in the nucleus, they function covered by nucleosomes in the form of minichromosomes. We did not expect too significant colocalization of p204 with viral genomes. However, MPyV genomes may overcome the restriction owing to the absence of nucleosomes in the regulatory region that includes sequences for transcription regulation and the ORI [14–16]. Indeed, we revealed that p204 interacts with replicating MPyV genomes (EdU-labeled viral DNA) and with the early viral LT antigen shown to bind the ORI region to promote viral replication. We cannot exclude that during replication, transcription, or repair processes, partial removal of histones from genomes can contribute to p204 sensing.

The activation of p204 during MPyV DNA sensing could involve post-translational modifications and/or

complexation with other molecules. During the recognition of herpesvirus genomes, the formation of a protein complex between IFI16, BRCA1 [DNA damage responses (DDRs) protein], and the histone H2B plays a significant role in IFI16 activation [73,74]. In addition, the acetylation of p204, similar to that described for IFI16 in herpesvirus genome sensing, could also control shuttling of p204 between the cytoplasm and the nucleus during p204 activation [41,56]. Our preliminary results from a proximity ligation assay using antibodies against p204 and acetylated lysine revealed the acetylation of p204 and/or the formation of a complex of p204 and an acetylated protein in the nucleus of infected cells (Data not shown). Further experiments will be needed to determine the molecular mechanism through which the p204 protein activates STING. Efforts to investigate the role of p204 in *IFN*-β gene induction further have been hampered by the unavailability of anti-p204 antibodies applicable for immunoprecipitation experiments. Interestingly, although it has been described that IFI16 can sense pathogenic DNA in both the cytoplasm and the nucleus [32,33,42,45,75], p204 does not seem to contribute to the cytosolic sensing of MPyV genomes. We did not observe high subpopulation of p204 in the cytosol. Some sporadic spots of p204 seen in the cytosol (data not shown) could correspond to the acetylated protein(s) (data not shown) shuttling from the nucleus to the cytosol to activate STING.

Recently, a new noncanonical pathway for IFN induction has been described [76]. In this pathway, ubiquitinylated, but not phosphorylated, STING extensively activates NF-kB and only minimally activates IRF3. The noncanonical pathway is postulated to be induced by dsDNA breaks that recruit p53, IFI16, and TRAF6. In this study, we followed the classical pathway of p204 activation as we found: (a) that massive concomitant STING and IRF3 phosphorylation is induced by MPyV infection and (b) that in p204-knockdown cells, infection by MPyV results in a significant reduction in IFN-β production associated with a marked decrease in IRF3 phosphorylation. Nevertheless, the contribution of noncanonical pathway to the IFN response induced by MPyV needs to be explored. Indeed, DNA damage response is activated during replication of the MPyV genome.

We further investigated involvement of the DNA sensor cGAS in the sensing of MPyV genomes. Using cGAS KO experiments, we demonstrated that cGAS was essential for the induction of IFN response by MPyV. The multiple locations of viral and cellular DNA colocalizing with cGAS was intriguing and surprising. However, we detected production of 2′3′-cGAMP only in the cytosolic fraction and not in the nuclear fractions of infected cells, consistent with most studies confirming cGAS sensing of DNA, its activation, and 2′3′-cGAMP production in the cytosol [77–80]. The production of 2′3′-cGAMP as a result of DNA sensing in the nucleus has been described in only one study. The authors of this study showed that dendritic cells produce low levels of2′3′-cGAMP in response to the overexpression of cGAS fused with the NLS sequence [44]. Our results, despite detection of abundant presence of cGAS in the nucleus and its occasional colocalization with MPyV genomes (Fig. 7C), strongly support the cytosolic sensing of cGAS and underline the existence of a tight regulatory mechanism that prevents sensing of MPyV DNA by cGAS in the nucleus. The binding of cGAS to nucleosomes and post-translational modifications, such as phosphorylation and acetylation, are involved in the prevention of self-DNA sensing [48,53]. The presence of cGAS on the viral genomes can be explained by its engagement in DDRs activated during polyomavirus replication. It was recently shown that cGAS colocalizes with H2AX and PARP1 in sites of DNA ds breaks (DSBs). cGAS binding to the site of DSBs was shown to inhibit homologous recombination repair by disruption of the formation of the PARP1–TIMELESS complex and by preventing the loading of RAD51 [46,81].

An increasing number of studies shows that cGAS and IFI16, besides their direct function in DNA recognition, can interact and affect the activation of STING in the cytosol [43,60]. In the nucleus, cGAS was shown to interact with IFI16 bound to herpesvirus DNA and protect IFI16 from proteasomal degradation [57]. We did not observe any detectable difference in the levels of p204 protein in infected wt MEFs and cGAS KO MEFs (Fig. 10). We also were not able to detect complexes of cGAS and IFI16 proteins in infected or noninfected cells by coimmunoprecipitation assays (data not shown). We assumed that structural differences between human IFI16 and its mouse ortholog, p204, distinct properties of host cells, and differences in the arrangement of nucleosomes on DNA accounted for the different findings obtained in this study.

It is well established that cGAS senses in the cytoplasm self-originated DNA present in micronuclei and activates IFN response [82]. The formation of micronuclei is the result of chromosome mis-segregation caused by replication stress or chromosomal instability. It requires the completion of mitotic cell division. Nevertheless, the cells in interphase (as during MPyV infection) can also display signs of stress, such as chromatin herniation, lamina alterations, and DNA DSBs allocated in the nuclear envelop opening sites,

which result in the formation of nuclear blebs (micronucleus-like bodies). Once a micronucleus is formed, the nuclear envelope reseals rapidly, assisted by the ESCRT III membrane-remodeling machinery [83,84]. Micronucleus membranes are fragile and defects in their biochemical composition have been characterized [85]. Thus, micronucleus-like bodies, similar to micronuclei, may also have defects in membranes that make DNA accessible to cGAS sensing.

Cells infected with polyomaviruses have several characteristics supporting the formation of micronucleus-like bodies and leakage of DNA into the cytosol. Polyomaviruses induce host genome instability by the actions of their early regulatory proteins. They activate the host DDR to prolong the S-phase, but also have the ability to inhibit DDR downstream effectors, for example, by suppressing p53 to avoid untimely p53-induced apoptosis or senescence [86,87]. S-phase arrest induced by DDR enables exploitation of cellular DNA replication machinery for viral genome replication. Massive replication of viral genomes is accompanied by a large rearrangement and enlargement of the cell nucleus and nuclear envelope remodeling; membrane disruption may be caused by the viroporin properties of minor structural proteins of MPyV, VP2, and VP3. Specifically, viroporins may be responsible for the disruption of nuclear and ER membranes [20,88].

The induction of IFN type I by human JCPyV in human astrocytes or by BKPyV in microvascular endothelial (cells that are a potential BKPyV reservoir) has been described [89,90]. Our study represents the first effort to understand the molecular mechanisms that govern IFN induction in polyomavirus infections. Here, we presented two mechanisms of sensing of MPyV DNA, one through the interaction of p204 with viral genomes in the nucleus and the second in the cytosol by cGAS binding of DNA fragments leaked directly from the nucleus or sensing DNA accessible after membrane disruption of micronucleus-like bodies. The sensors p204 and cGAS appear to be activated independently by the virus during infection. Surprisingly, the production of IFN is moderate in MPyV-infected cells, suggesting a tight regulation of the IFN response by cells and by the intervention of viral antigens. The moderate IFN induction may contribute to polyomavirus persistency in the host.

Materials and methods

Cell lines and viruses

Mouse 3T6 fibroblasts (ATCC, Manassas, VA, USA; CCL-96), mouse embryo fibroblasts (MEFs) M-Fb-481 (Lonza, Basel, Switzerland), immortalized MEF-STING wt, MEF-STING KO, MEF-cGAS wt, and MEF-cGAS KO (kindly provided by J. Cambier, University of Colorado, USA, and J. Rehwinkel, University of Oxford, UK) were grown at 37 °C in a humidified incubator with an atmosphere of 5% CO_2, using Dulbecco's modified Eagle's medium (DMEM) from Sigma-Aldrich (St. Louis, MO, USA) supplemented with 10% fetal bovine serum (Invitrogen, Waltham, MA, USA) and 4 mM L-glutamine (Invitrogen). The MPyV strain BG (GenBank: AF442959.1) was isolated and purified from infected 3T6 cells using the standard protocol for purification by CsCl [91]. Mutant viruses lacking the NLS in capsid proteins (MPyVΔNLS: VP1K6Q-S7R-G8R-VP2/VP3 K314A-K315A-R317A) were prepared as described in [23]. In detail, a pMJG plasmid containing the entire genome of MPyV BG strain was used for mutagenesis. Next, the mutated or wt genomes were used for the transfection of 3T6 cells. After transfection, viruses were purified as described above [91] and purity of preparations was followed by electron microscopy using negative staining as described before [23].

Generation of 3T6 cell line expressing GFP-cGAS

For the production of N-terminally eGFP-tagged mouse cGAS, the plasmid pMSCVpuro-eGFP-mcGAS, coding for GFP-cGAS (gift from Andrew Jackson & Martin Reijns—plasmid # 108675 from Addgene, Watertown, MA, USA) [82], was transfected using Lipofectamine into Phoenix Ecotropic cells for the production of the retrovirus. Then, the retrovirus was used for transduction of 3T6 cells in the presence of polybrene. Mouse cells were further selected for stable integration using 1–10 $\mu g \cdot mL^{-1}$ puromycin.

Viral genome quantification

The quantification of MPyV genomes was performed by real-time PCR assay using iQ™ SYBR® Green Supermix (Bio-Rad Laboratories, Hercules, CA, USA), as described in [23]. The primer sets used were: VP1, 5′-GCAAGAAGGCGACGAC-3′ and 5′-TGGCCTCCCTCATAAGT-3′; and LT 5′-GCTGACAAAGAAAGGCTGCT-3′ and 5′-AGCCGGTTCCTCCTAGATTC-3′.

Reverse transcription quantitative PCR

Total cellular RNA was extracted using High Pure RNA Isolation Kit (Roche, Penzberg, Upper Bavaria, Germany) in accordance with the manufacturer's protocol. The RNA concentration and purity were measured by a nanodrop spectrophotometer (Thermo Fisher Scientific, Waltham, MA, USA). Reverse transcription was performed using the iScriptcDNA synthesis kit (Bio-Rad Laboratories) in accordance with the manufacturer's instructions. cDNAs were amplified by PCR using the following primer sets:

MX-1, 5′-GGTCGGCTTCTGGTTTTGTA-3′ and 5′-GAACAGGTCCACTTCCTCCA-3′;

GAPDH, 5′-ATGACATCAAGAAGGTGGTG-3′ and 5′-ATACCAGGAAATGAGCTTG-3′;

IFN-β, 5′-CCCTATGGAGATGACGGAGA-3′ and 5′-CTGTCTGCTGGTGGAGTTCA-3′;

spliced *LT*, 5′-GAACCGGCTTCCAGGGCTC-3′ and 5′-CTTAGGCGGCGACTGGTAG-3′.

The quantification of PCR products in real-time was performed in a LightCycler 480 II (Roche) using the LightCycler® 480 SYBR Green I Master kit (Roche) in accordance with the manufacturer's protocol. The quantification of target gene expression was performed using LightCycler 480 II software based on the relative quantification method, which determined the concentration of target amplicons normalized to the reference gene GAPDH.

SDS/PAGE and western blotting analysis

The cells were harvested and then resuspended in modified RIPA buffer (10 mM Tris/HCl, pH 7.4, 1 mM EDTA, 150 mM NaCl, 1% Nonidet P-40, 1% sodium deoxycholate, 0.1% SDS) supplemented with protease inhibitor cocktail (Complete Mini EDTA free from Roche). Then, the cells were lysed in RIPA for 20 min on ice and cell debris was removed by centrifugation. The proteins were resuspended in Laemmli buffer and separated by 10% SDS/PAGE. The gels were blotted to nitrocellulose membranes and immunoassayed using the indicated antibodies. The proteins were visualized by chemiluminescence using the application of AI-600 (GE Healthcare, Chicago, IL, USA).

Nuclear-cytoplasmic fractionation

We used either the nuclear and cytosol extraction kit to prepare cell fractions in accordance with the manufacturer's instructions (G-Biosciences, Saint Louis, MO, USA) or performed extraction using NP40 in accordance with the protocol described by Nabbi *et al.* [92]. In addition, when required, nuclear fractions were further separated into soluble and insoluble fractions. Nuclear fraction was resuspended in Solution B (3 mM EDTA, 0.2 mM EGTA, and 1 mM DTT) and incubated on ice for 30 min. The soluble fraction was separated by centrifugation at 1700 ***g*** for 4 min at 4 °C. The pellet containing chromatin was washed with Buffer B, and the chromatin pellet was lysed in RIPA buffer.

Antibodies

Rat monoclonal anti-large T antigen (LT; provided by B. E. Griffin, Imperial College of Science, Technology and Medicine at St. Mary's, London, UK), rabbit polyclonal antibody against GAPDH (Sigma-Aldrich), rabbit polyclonal anti-phospho-IRF3 (Ser369(4D4G); Cell Signaling Technology, Danvers, MA, USA), rabbit polyclonal anti-phospho-IRF3 (Ser369 (D601M); Cell Signaling Technology), rabbit polyclonal anti-phospho-STING-Ser365-D8F4W (Cell Signaling Technology), rabbit polyclonal anti-phospho-STING (Ser365(D1C4T); Cell Signaling Technology), rabbit polyclonal against IFI16/p204 (Elabscience, Houston, TX, USA), rabbit polyclonal anti STING/anti MPYS (Sigma), rabbit monoclonal anti cGAS (Cell Signaling Technology), polyclonal rabbit anti-biotin antibody (A150; Bethyl Laboratories, Montgomery, TX USA), rabbit IgG-HRP (Bio-Rad), goat anti-rat IgG-HRP (Bio-Rad), Cy3® goat anti-rabbit IgG (Thermo Fisher Scientific), Alexa Fluor® 488 goat anti-rabbit IgG (Thermo Fisher Scientific), Alexa Fluor® 488 goat anti-rat IgG (Thermo Fisher Scientific), Alexa Fluor® 488 goat anti-rabbit (Cell Signaling Technology), and Alexa Fluor® 647 goat anti-rat IgG (Thermo Fisher Scientific).

Immunofluorescence staining

The cells were grown on coverslips. At the indicated time points, the cells were fixed in 4% paraformaldehyde (PFA) for 15 min or ice-cold methanol for 10 min at −20 °C and permeabilized with 0.5% Triton X-100 in PBS for 5 min (after fixation with PFA). After washing in PBS, the cells were incubated with blocking solution (0.25% BSA and 0.25% porcine skin gelatin in PBS) for 30 min. Immunostaining was conducted with primary and secondary antibodies for 1 h and 30 min, respectively, with extensive washing in 1× PBS after each incubation.

The coverslips were stained with DAPI, mounted on droplets of Anti-Fade Fluorescence Mounted Medium (Abcam, Cambridge, UK), and images were obtained using a LSM 880NLO confocal microscope (Carl Zeiss, Oberkochen, Germany).

Immunofluorescence staining with pre-extraction buffer

Cells were grown on coverslips. At the indicated time points, the medium was removed, and the cells were incubated for 5 min on ice with pre-extraction buffer containing 25 mM HEPES, 50 mM NaCl, 3 mM $MgCl_2$, 300 mM sucrose, and 0.5% Triton X-100 (pH 7.4). The cells were then washed once with 1× PBS and fixed with ice-cold methanol for 10 min at −20 °C. After washing in PBS, cells were incubated for 30 min in blocking buffer, as above, and the staining was performed as for regular immunofluorescence staining (as described above).

Fluorescence *in situ* hybridization combined with immunofluorescence or Edu labeling

We performed FISH in combination with immunofluorescence in accordance with the protocol described by Solovei and Cremer [93]. In brief, cells were grown on coverslips,

fixed with 2% PFA for 10 min, permeabilized with 0.5% Triton X-100 for 10 min, incubated in blocking solution (1% BSA/PBS) for 1 h, and stained by the selected antibodies or subjected to Edu Click chemistry. The cells were postfixed with 4% PFA for 5 min, treated with RNAse, and incubated with 20% glycerol/PBS for 1 h. Then, five freeze-thaw cycles were performed in liquid nitrogen. The cells were then equilibrated in 50% formamide/2× SSC for 8 h and hybridized with the MPyV DNA probe generated by nick translation using BioNick DNA Labeling System (Invitrogen). Denaturation and hybridization were performed as follows: 90 °C-2 min, 80 °C-2 min, 70 °C-2 min, 60 °C-2 min, 50 °C-2 min, 42 °C-1 h, and 37 °C overnight. After hybridization, the cells were washed three times in 2× SSC at 37 °C and twice in 0.1× SSC at 60 °C. Each wash step was performed for 10 min. After washing, the cells were incubated with blocking solution (1% BSA/PBS) for 1 h and processed for the detection of biotin by using antibodies. Coverslips were stained with DAPI and mounted on droplets of Anti-Fade Fluorescence Mounted Medium (Abcam). Images were obtained using a LSM 880NLO confocal microscope (Carl Zeiss).

Viral infection

Cells were seeded on 13-mm glass coverslips or plates and grown to a confluency of approximately 50%. On the day of infection, the cells were washed with serum-free DMEM and incubated with MPyV diluted in serum-free medium for 1 h at 37 °C. The start of infection was measured from the time the virus was added to cells. After virus adsorption, the cells were washed to remove the unbound virus and incubated in DMEM supplemented with 10% FBS for the indicated times.

Cell stimulation with inducers of IFN

Polyinosinic:polycytidylic acid (GE Healthcare) was used to stimulate 3T6 cells; specifically, 2×10^6 cells were transfected by TurboFect (Thermo Fisher Scientific) with 20 μg of poly (I:C). The cells were incubated for 16 h and then collected for isolation of RNA or for the preparation of cell lysates. c-di-GAMP (InvivoGen, San Diego, CA, USA), pDNA, CpG oligonucleotide (InvivoGen) or 26-mer DNA (G3-YSD, InvivoGen) were used to stimulate 3T6 cells as follows: cells (4×10^6) were transfected with 4 μg of c-di-GAMP, 6 μg of pDNA, or 4 μg CpG by Amaxa nucleofector (Lonza), incubated for a further 6 h, and collected for the isolation of RNA.

EdU click chemistry

The Click-iT EdU reaction was performed in accordance with the instructions for the Click-iT imaging kit (Invitrogen). In brief, a solution of 20 μM EdU was prepared in complete medium and added to growing cells on coverslips to a final concentration of 10 μM. After incubation for 30 min, the cells were fixed, permeabilized, blocked in 3% BSA/PBS, and subjected to Click-iT reaction.

siRNA transfection

Sense and antisense siRNA for p204 were prepared in Lipofectamine in accordance with manufacturer's instructions (Thermo Fisher Scientific). The siRNA sequences were: 5′-GUUUCAUCAAGAUAUCAAAtt-3′ and 5′-UUUGAUAUCUUGAUGAAAtg-3′. As a control, the Silencer® Select Negative Control #1 siRNA (Thermo Fisher Scientific) was used.

2′3′-cGAMP detection by LC-MS

For detection of 2′3′-cGAMP, the cells were detached using trypsin and 4×10^6 cells were collected and used for the experiment. The cells were washed five times with 1 mL of 1× PBS and lysed in lysis buffer (20% acetonitrile and 40% methanol in deionized water). Then, the lysates were heated for 10 min at 60 °C and cooled for 10 min on ice. After cooling, the samples were centrifuged at 17 000 ***g*** for 10 min at 4 °C, and the supernatant was collected in a clean Eppendorf tube (Supernatant A). The pellet produced in the previous centrifuge step was washed in 500 μL of H_2O and centrifuged at 17 000 ***g*** for 10 min at 4 °C, and the supernatant was collected in a clean Eppendorf tube (Supernatant B). Supernatants A and B were combined and centrifuged at 17 000 ***g*** for 5 min at 4 °C and transferred to a new Eppendorf tube. To prepare the samples for analysis by LC-MS, the samples were frozen at −80 °C for 1 day, dried by vacuum centrifugation, and resuspended in 40 μL of H_2O.

As control, an internal standard of 100 pmol of 2′3′-cGAMP was spiked into the lysate of mock-infected cells or cells transfected with a pDNA and collected after 2 h.

2′3′-cGAMP expression was measured using a Dionex Ultimate 3000RS LC system coupled to a TSQ Quantiva mass spectrometer (Thermo Fisher Scientific) using an ESI source in positive mode with the following ion source parameters: ion transfer tube temperature, 300 °C; vaporizer temperature, 125 °C; spray voltage, 3500 V; sheath gas, 35 arbitrary units (au); auxiliary gas, 5 au. A ZIC®-HILIC column (150 mm × 2.1 mm, 5 μm) from Merck (Darmstadt, Germany) was used to separate the analytes. The column was maintained at room temperature and an injection volume of 2 μL was used per sample. A gradient elution was set from 15% B to 60% B (A: 95% acetonitrile and 5% 10 mM ammonium acetate pH 9.3, B: 10 mM ammonium carbonate in water, pH 9.3) in 7.3 min at a flow rate of 200 $\mu L \cdot min^{-1}$, followed by a washing phase (2.7 min of 60% B) and an equilibration phase (9 min of 15% B). For the targeted determination of 2′3′-cGAMP,

a selective reaction monitoring assay was used, which was developed previously, comprising infusion of the pure compound and monitoring the following seven transitions: 675.1 > 136.1, 675.1 > 524.1, 675.1 > 312.1, 675.1 > 506.0, 675.1 > 152.1, 675.1 > 476.0, and 675.1 > 330.0. The integration of 2′3′-cGAMP peak areas was related to the transition 675.1 > 506, which provided appropriate signal intensity and was less affected by the matrix effect.

2′3′-cGAMP ELISA detection

2′3′-cGAMP ELISA was performed in accordance with the manufacturer's protocol using 2′3′-cGAMP ELISA Kit (Arbor Assays, Ann Arbor, MI, USA). In brief, mock-infected or infected cells, (1.5×10^6) were used for fractionation with the kit described above. The fractions were handled on ice and immediately used for ELISA. The 2′3′-cGAMP standards were prepared in the cytosolic and nuclear cell lysis buffers to achieve precise calculation of the 2′3′-cGAMP concentration in the samples. The cell fractions or standards were added to the ELISA plates, followed by antibodies against 2′3′-cGAMP and HRP-labeled–2′3′-cGAMP for a competition assay. After incubation for 2 h, the plates were washed; subsequently, the reaction was developed using TMB and stopped by HCl. The optical density (OD) was measured at 450 nm using a microplate ELISA reader (Tecan, Männedorf, Switzerland). The data were processed using the Four Parameter logistic (4PL) curve calculator available online (myassays.com) as recommended by the manufacturer.

Statistical analysis

Student's *t*-test was performed using the GRAPHPAD PRISM software, version 6.0 (GraphPad Software, La Jolla, CA, USA). Asterisks indicate *P*-values representing statistically significant differences ($*P \leq 0.05$, $**P \leq 0.01$, $***P \leq 0.001$, $****P \leq 0.0001$).

Acknowledgements

We are grateful to the Imaging Methods Core Facility at BIOCEV [supported by the MEYS CR (Large RI Project LM2018129 Czech-Bioimaging) and ERDF (project No. CZ.02.1.01/0.0/0.0/18_046/0016045)] for their support with obtaining the imaging data presented in this paper, as well to the Proteomic and Metabolomic Core Facility, BIOCEV, Faculty of Science, Charles University in Prague (supported by OP VaVpI CZ.1.05/1.1.00/02.0109) for the mass spectrometric measurements. This study was supported by the Grant Agency of the Czech Republic (19-14445S) and by the specific university research project grant-SVV by the Charles University (SVV 260568).

Author contributions

SH, BR, IS, VS, and JF contributed to conception and design of the experiments. BR, IS, SH, and VS performed the experiments. BR, SH, JF, IS, and VS analyzed the data. SH, JF, BR, and IS wrote the manuscript.

Conflict of interest

The authors declare no conflict of interest.

Peer Review

The peer review history for this article is available at https://publons.com/publon/10.1111/febs.15962.

References

1 Cook L (2016) Polyomaviruses. *Microbiol Spectr* **4**, 3–9.
2 Gheit T, Dutta S, Oliver J, Robitaille A, Hampras S, Combes J-D, McKay-Chopin S, Le Calvez-Kelm F, Fenske N, Cherpelis B *et al.* (2017) Isolation and characterization of a novel putative human polyomavirus. *Virology* **506**, 45–54.
3 Feng H, Shuda M, Chang Y & Moore PS (2008) Clonal integration of a polyomavirus in human merkel cell carcinoma. *Science* **319**, 1096–1100.
4 Gardner SD, Field AM, Coleman DV & Hulme B (1971) New human papovavirus (B.K.) isolated from urine after renal transplantation. *Lancet* **1**, 1253–1257.
5 van der Meijden E, Janssens RWA, Lauber C, Bouwes Bavinck JN, Gorbalenya AE & Feltkamp MCW (2010) Discovery of a new human polyomavirus associated with trichodysplasia spinulosa in an immunocompromized patient. *PLoS Pathog* **6**, e1001024.
6 Padgett BL, Walker DL, ZuRhein GM, Eckroade RJ & Dessel BH (1971) Cultivation of papova-like virus from human brain with progressive multifocal leucoencephalopathy. *Lancet* **1**, 1257–1260.
7 Viscidi RP, Rollison DE, Sondak VK, Silver B, Messina JL, Giuliano AR, Fulp W, Ajidahun A & Rivanera D (2011) Age-specific seroprevalence of merkel cell polyomavirus, BK Virus, and JC virus. *Clin Vaccine Immunol* **18**, 1737–1743.
8 Hampras SS, Giuliano AR, Lin H-Y, Fisher KJ, Abrahamsen ME, McKay-Chopin S, Gheit T, Tommasino M & Rollison DE (2015) Natural history of polyomaviruses in men: the HPV infection in men (HIM) Study. *J Infect Dis* **211**, 1437–1446.
9 Nicol JTJ, Robinot R, Carpentier A, Carandina G, Mazzoni E, Tognon M, Touzé A & Coursaget P (2013) Age-specific seroprevalences of merkel cell polyomavirus, human polyomaviruses 6, 7, and 9, and

trichodysplasia spinulosa-associated polyomavirus. *Clin Vaccine Immunol* **20**, 363–368.
10 Qin Q, EL Shwetank F, Maru S & Lukacher AE (2016) Type I interferons regulate the magnitude and functionality of mouse polyomavirus-specific CD8 T cells in a virus strain-dependent manner. *J Virol* **90**, 5187–5199.
11 Chen XS (1998) Interaction of polyomavirus internal protein VP2 with the major capsid protein VP1 and implications for participation of VP2 in viral entry. *EMBO J* **17**, 3233–3240.
12 Stehle T & Harrison SC (1996) Crystal structures of murine polyomavirus in complex with straight-chain and branched-chain sialyloligosaccharide receptor fragments. *Structure* **4**, 183–194.
13 Carmichael G (2016) Gene regulation and quality control in murine polyomavirus infection. *Viruses* **8**, 284.
14 Jakobovits EB, Bratosin S & Aloni Y (1980) A nucleosome-free region in SV40 minichromosomes. *Nature* **285**, 263–265.
15 Saragosti S, Moyne G & Yaniv M (1980) Absence of nucleosomes in a fraction of SV40 chromatin between the origin of replication and the region coding for the late leader RNA. *Cell* **20**, 65–73.
16 Varshavsky AJ, Sundin O & Bohn M (1979) A stretch of "late" SV40 viral DNA about 400 bp long which includes the origin of replication is specifically exposed in SV40 minichromosomes. *Cell* **16**, 453–466.
17 Liebl D, Difato F, Hornikova L, Mannova P, Stokrova J & Forstova J (2006) Mouse polyomavirus enters early endosomes, requires their acidic pH for productive infection, and meets transferrin cargo in Rab11-positive endosomes. *J Virol* **80**, 4610–4622.
18 Qian M, Cai D, Verhey KJ & Tsai B (2009) A lipid receptor sorts polyomavirus from the endolysosome to the endoplasmic reticulum to cause infection. *PLoS Pathog* **5**, e1000465.
19 Zila V, Difato F, Klimova L, Huerfano S & Forstova J (2014) Involvement of microtubular network and its motors in productive endocytic trafficking of mouse polyomavirus. *PLoS One* **9**, e96922.
20 Huérfano S, Ryabchenko B, Španielová H & Forstová J (2017) Hydrophobic domains of mouse polyomavirus minor capsid proteins promote membrane association and virus exit from the ER. *FEBS J* **284**, 883–902.
21 Inoue T & Tsai B (2011) A large and intact viral particle penetrates the endoplasmic reticulum membrane to reach the cytosol. *PLoS Pathog* **7**, e1002037.
22 Magnuson B, Rainey EK, Benjamin T, Baryshev M, Mkrtchian S & Tsai B (2005) ERp29 triggers a conformational change in polyomavirus to stimulate membrane binding. *Mol Cell* **20**, 289–300.
23 Soldatova I, Prilepskaja T, Abrahamyan L, Forstová J & Huérfano S (2018) Interaction of the mouse polyomavirus capsid proteins with importins is required for efficient import of viral DNA into the cell nucleus. *Viruses* **10**, 165.
24 Chen L & Fluck M (2001) Kinetic analysis of the steps of the polyomavirus lytic cycle. *J Virol* **75**, 8368–8379.
25 Ahmad-Nejad P, Häcker H, Rutz M, Bauer S, Vabulas RM & Wagner H (2002) Bacterial CpG-DNA and lipopolysaccharides activate Toll-like receptors at distinct cellular compartments. *Eur J Immunol* **32**, 1958.
26 Bauer S, Kirschning CJ, Hacker H, Redecke V, Hausmann S, Akira S, Wagner H & Lipford GB (2001) Human TLR9 confers responsiveness to bacterial DNA via species-specific CpG motif recognition. *Proc Natl Acad Sci USA* **98**, 9237–9242.
27 Hemmi H, Takeuchi O, Kawai T, Kaisho T, Sato S, Sanjo H, Matsumoto M, Hoshino K, Wagner H, Takeda K *et al.* (2000) A Toll-like receptor recognizes bacterial DNA. *Nature* **408**, 740–745.
28 Takaoka A, Wang Z, Choi MK, Yanai H, Negishi H, Ban T, Lu Y, Miyagishi M, Kodama T, Honda K *et al.* (2007) DAI (DLM-1/ZBP1) is a cytosolic DNA sensor and an activator of innate immune response. *Nature* **448**, 501–505.
29 Chiu Y-H, MacMillan JB & Chen ZJ (2009) RNA polymerase III detects cytosolic DNA and induces Type I interferons through the RIG-I pathway. *Cell* **138**, 576–591.
30 Hornung V, Ablasser A, Charrel-Dennis M, Bauernfeind F, Horvath G, DanielR C, Latz E & Fitzgerald KA (2009) AIM2 recognizes cytosolic dsDNA and forms a caspase-1-activating inflammasome with ASC. *Nature* **458**, 514–518.
31 Horan KA, Hansen K, Jakobsen MR, Holm CK, Soby S, Unterholzner L, Thompson M, West JA, Iversen MB, Rasmussen SB *et al.* (2013) Proteasomal degradation of herpes simplex virus capsids in macrophages releases DNA to the cytosol for recognition by DNA sensors. *J Immunol* **190**, 2311–2319.
32 Unterholzner L, Keating SE, Baran M, Horan KA, Jensen SB, Sharma S, Sirois CM, Jin T, Latz E, Xiao TS *et al.* (2010) IFI16 is an innate immune sensor for intracellular DNA. *Nat Immunol* **11**, 997–1004.
33 Zhu W, Liu P, Yu L, Chen Q, Liu Z, Yan K, Lee WM, Cheng CY & Han D (2014) p204-Initiated Innate Antiviral Response in Mouse Leydig Cells1. *Biol Reprod* **91**.
34 Yang P, An H, Liu X, Wen M, Zheng Y, Rui Y & Cao X (2010) The cytosolic nucleic acid sensor LRRFIP1 mediates the production of type I interferon via a β-catenin-dependent pathway. *Nat Immunol* **11**, 487–494.
35 Zhang X, Brann TW, Zhou M, Yang J, Oguariri RM, Lidie KB, Imamichi H, Huang D-W, Lempicki RA, Baseler MW *et al.* (2011) Cutting edge: Ku70 is a novel cytosolic DNA sensor that induces type III rather than type I IFN. *J Immunol* **186**, 4541–4545.

36 Kim T, Pazhoor S, Bao M, Zhang Z, Hanabuchi S, Facchinetti V, Bover L, Plumas J, Chaperot L, Qin J *et al.* (2010) Aspartate-glutamate-alanine-histidine box motif (DEAH)/RNA helicase A helicases sense microbial DNA in human plasmacytoid dendritic cells. *Proc Natl Acad Sci USA* **107**, 15181–15186.
37 Zhang Z, Yuan B, Bao M, Lu N, Kim T & Liu Y-J (2011) The helicase DDX41 senses intracellular DNA mediated by the adaptor STING in dendritic cells. *Nat Immunol* **12**, 959–965.
38 Sun L, Wu J, Du F, Chen X & Chen ZJ (2013) Cyclic GMP-AMP synthase is a cytosolic DNA sensor that activates the type I interferon pathway. *Science* **339**, 786–791.
39 Wu J, Sun L, Chen X, Du F, Shi H, Chen C & Chen ZJ (2013) Cyclic GMP-AMP is an endogenous second messenger in innate immune signaling by cytosolic DNA. *Science* **339**, 826–830.
40 Diner BA, Li T, Greco TM, Crow MS, Fuesler JA, Wang J & Cristea IM (2015) The functional interactome of PYHIN immune regulators reveals IFIX is a sensor of viral DNA. *Mol Syst Biol* **11**, 787.
41 Li T, Diner BA, Chen J & Cristea IM (2012) Acetylation modulates cellular distribution and DNA sensing ability of interferon-inducible protein IFI16. *Proc Natl Acad Sci USA* **109**, 10558–10563.
42 Orzalli MH, DeLuca NA & Knipe DM (2012) Nuclear IFI16 induction of IRF-3 signaling during herpesviral infection and degradation of IFI16 by the viral ICP0 protein. *Proc Natl Acad Sci USA* **109**, E3008–E3017.
43 Storek KM, Gertsvolf NA, Ohlson MB & Monack DM (2015) cGAS and Ifi204 cooperate to produce type I IFNs in response to *Francisella* Infection. *J Immunol* **194**, 3236–3245.
44 Gentili M, Lahaye X, Nadalin F, Nader GPF, Puig Lombardi E, Herve S, De Silva NS, Rookhuizen DC, Zueva E, Goudot C *et al.* (2019) The N-terminal domain of cGAS determines preferential association with centromeric DNA and innate immune activation in the nucleus. *Cell Rep* **26**, 2377–2393.e13.
45 Stratmann SA, Morrone SR, van Oijen AM & Sohn J 2015) The innate immune sensor IFI16 recognizes foreign DNA in the nucleus by scanning along the duplex. *eLife* **4**, e11721.
46 Liu H, Zhang H, Wu X, Ma D, Wu J, Wang L, Jiang Y, Fei Y, Zhu C, Tan R *et al.* (2018) Nuclear cGAS suppresses DNA repair and promotes tumorigenesis. *Nature* **563**, 131–136.
47 Seo GJ, Kim C, Shin W-J, Sklan EH, Eoh H & Jung JU (2018) TRIM56-mediated monoubiquitination of cGAS for cytosolic DNA sensing. *Nat Commun* **9**, 613.
48 Song B, Greco TM, Lum KK, Taber CE & Cristea IM (2020) The DNA sensor cGAS is decorated by acetylation and phosphorylation modifications in the context of immune signaling. *Mol Cell Proteomics* **19**, 1193–1208.
49 Volkman HE, Cambier S, Gray EE & Stetson DB (2019) Tight nuclear tethering of cGAS is essential for preventing autoreactivity. *eLife* **8**, e47491.
50 Morrone SR, Wang T, Constantoulakis LM, Hooy RM, Delannoy MJ & Sohn J (2014) Cooperative assembly of IFI16 filaments on dsDNA provides insights into host defense strategy. *Proc Natl Acad Sci USA* **111**, E62–E71.
51 Seo GJ, Yang A, Tan B, Kim S, Liang Q, Choi Y, Yuan W, Feng P, Park H-S & Jung JU (2015) Akt kinase-mediated checkpoint of cGAS DNA sensing pathway. *Cell Rep* **13**, 440–449.
52 Ni X, Ru H, Ma F, Zhao L, Shaw N, Feng Y, Ding W, Gong W, Wang Q, Ouyang S *et al.* (2016) New insights into the structural basis of DNA recognition by HINa and HINb domains of IFI16. *J Mol Cell Biol* **8**, 51–61.
53 Kujirai T, Zierhut C, Takizawa Y, Kim R, Negishi L, Uruma N, Hirai S, Funabiki H & Kurumizaka H (2020) Structural basis for the inhibition of cGAS by nucleosomes. *Science* **370**, 455–458.
54 Xia P, Ye B, Wang S, Zhu X, Du Y, Xiong Z, Tian Y & Fan Z (2016) Glutamylation of the DNA sensor cGAS regulates its binding and synthase activity in antiviral immunity. *Nat Immunol* **17**, 369–378.
55 Dai J, Huang Y-J, He X, Zhao M, Wang X, Liu Z-S, Xue W, Cai H, Zhan X-Y, Huang S-Y *et al.* (2019) Acetylation blocks cGAS activity and inhibits self-DNA-induced autoimmunity. *Cell* **176**, 1447–1460.e14.
56 Ansari MA, Dutta S, Veettil MV, Dutta D, Iqbal J, Kumar B, Roy A, Chikoti L, Singh VV & Chandran B (2015) Herpesvirus genome recognition induced acetylation of nuclear IFI16 is essential for its cytoplasmic translocation, inflammasome and IFN-β responses. *PLOS Pathog* **11**, e1005019.
57 Orzalli MH, Broekema NM, Diner BA, Hancks DC, Elde NC, Cristea IM & Knipe DM (2015) cGAS-mediated stabilization of IFI16 promotes innate signaling during herpes simplex virus infection. *Proc Natl Acad Sci USA* **112**, E1773–E1781.
58 Fan X, Jiang J, Zhao D, Chen F, Ma H, Smith P, Unterholzner L, Xiao TS & Jin T (2021) Structural mechanism of DNA recognition by the p204 HIN domain. *Nucleic Acids Res* **49**, 2959–2972.
59 Lum KK, Howard TR, Pan C & Cristea IM (2019) Charge-mediated pyrin oligomerization nucleates antiviral IFI16 sensing of herpesvirus DNA. *MBio* **10**, e01428-19.
60 Almine JF, O'Hare CAJ, Dunphy G, Haga IR, Naik RJ, Atrih A, Connolly DJ, Taylor J, Kelsall IR, Bowie AG *et al.* (2017) IFI16 and cGAS cooperate in the activation of STING during DNA sensing in human keratinocytes. *Nat Commun* **8**, 14392.

61 Liu S, Cai X, Wu J, Cong Q, Chen X, Li T, Du F, Ren J, Wu Y-T, Grishin NV *et al.* (2015) Phosphorylation of innate immune adaptor proteins MAVS, STING, and TRIF induces IRF3 activation. *Science* **347**, aaa2630.
62 Gao P, Ascano M, Wu Y, Barchet W, Gaffney BL, Zillinger T, Serganov AA, Liu Y, Jones RA, Hartmann G *et al.* (2013) Cyclic [G(2′,5′)pA(3′,5′)p] is the metazoan second messenger produced by DNA-activated cyclic GMP-AMP synthase. *Cell* **153**, 1094–1107.
63 Huerfano S, Ryabchenko B & Forstová J (2013) Nucleofection of expression vectors induces a robust interferon response and inhibition of cell proliferation. *DNA Cell Biol* **32**, 467–479.
64 Semenova N, Bosnjak M, Markelc B, Znidar K, Cemazar M & Heller L (2019) Multiple cytosolic DNA sensors bind plasmid DNA after transfection. *Nucleic Acids Res* **47**, 10235–10246.
65 Hua K & Ferland RJ (2017) Fixation methods can differentially affect ciliary protein immunolabeling. *Cilia* **6**, 5.
66 Ma Z, Ni G & Damania B (2018) Innate sensing of DNA virus genomes. *Annu Rev Virol* **5**, 341–362.
67 Carbone M, Ascione G, Chichiarelli S, Garcia M-I, Eufemi M & Amati P (2004) Chromosome-Protein interactions in polyomavirus virions . *J Virol* **78**, 513–519.
68 Jiang M, Abend JR, Tsai B & Imperiale MJ (2009) Early events during BK virus entry and disassembly. *J Virol* **83**, 1350–1358.
69 Sun C, Luecke S, Bodda C, Jønsson KL, Cai Y, Zhang B-C, Jensen SB, Nordentoft I, Jensen JM, Jakobsen MR *et al.* (2019) Cellular requirements for sensing and elimination of incoming HSV-1 DNA and capsids. *J Interferon Cytokine Res* **39**, 191–204.
70 Kumar S, Morrison JH, Dingli D & Poeschla E (2018) HIV-1 activation of innate immunity depends strongly on the intracellular level of TREX1 and sensing of incomplete reverse transcription products. *J Virol* **92**, e00001–18.
71 Herrera FJ & Triezenberg SJ (2004) VP16-dependent association of chromatin-modifying coactivators and underrepresentation of histones at immediate-early gene promoters during herpes simplex virus infection. *J Virol* **78**, 9689–9696.
72 Oh J & Fraser NW (2008) Temporal association of the herpes simplex virus genome with histone proteins during a lytic infection. *J Virol* **82**, 3530–3537.
73 Dutta D, Dutta S, Veettil MV, Roy A, Ansari MA, Iqbal J, Chikoti L, Kumar B, Johnson KE & Chandran B (2015) BRCA1 regulates IFI16 mediated nuclear innate sensing of herpes viral DNA and subsequent induction of the innate inflammasome and interferon-β responses. *PLoS Pathog* **11**, e1005030.
74 Iqbal J, Ansari MA, Kumar B, Dutta D, Roy A, Chikoti L, Pisano G, Dutta S, Vahedi S, Veettil MV *et al.* (2016) Histone H2B-IFI16 recognition of nuclear herpesviral genome induces cytoplasmic interferon-β responses. *PLoS Pathog* **12**, e1005967.
75 Diner BA, Lum KK, Toettcher JE & Cristea IM (2016) Viral DNA sensors IFI16 and cyclic GMP-AMP synthase possess distinct functions in regulating viral gene expression, immune defenses, and apoptotic responses during herpesvirus, infection. *MBio* **7**, e01553-16.
76 Dunphy G, Flannery SM, Almine JF, Connolly DJ, Paulus C, Jønsson KL, Jakobsen MR, Nevels MM, Bowie AG & Unterholzner L (2018) Non-canonical activation of the DNA sensing adaptor STING by ATM and IFI16 mediates NF-κB signaling after nuclear DNA damage. *Mol Cell* **71**, 745–760.e5.
77 Ablasser A, Goldeck M, Cavlar T, Deimling T, Witte G, Röhl I, Hopfner K-P, Ludwig J & Hornung V (2013) cGAS produces a 2′-5′-linked cyclic dinucleotide second messenger that activates STING. *Nature* **498**, 380–384.
78 Glück S, Guey B, Gulen MF, Wolter K, Kang T-W, Schmacke NA, Bridgeman A, Rehwinkel J, Zender L & Ablasser A (2017) Innate immune sensing of cytosolic chromatin fragments through cGAS promotes senescence. *Nat Cell Biol* **19**, 1061–1070.
79 Chen Q, Sun L & Chen ZJ (2016) Regulation and function of the cGAS–STING pathway of cytosolic DNA sensing. *Nat Immunol* **17**, 1142–1149.
80 Zierhut C, Yamaguchi N, Paredes M, Luo J-D, Carroll T & Funabiki H (2019) The Cytoplasmic DNA sensor cGAS promotes mitotic cell death. *Cell* **178**, 302–315.e23.
81 Jiang H, Xue X, Panda S, Kawale A, Hooy RM, Liang F, Sohn J, Sung P & Gekara NO (2019) Chromatin-bound cGAS is an inhibitor of DNA repair and hence accelerates genome destabilization and cell death. *EMBO J* **38**, e102718.
82 Mackenzie KJ, Carroll P, Martin C-A, Murina O, Fluteau A, Simpson DJ, Olova N, Sutcliffe H, Rainger JK, Leitch A *et al.* (2017) cGAS surveillance of micronuclei links genome instability to innate immunity. *Nature* **548**, 461–465.
83 Cheong HSJ, Seth I, Joiner MC & Tucker JD (2013) Relationships among micronuclei, nucleoplasmic bridges and nuclear buds within individual cells in the cytokinesis-block micronucleus assay. *Mutagenesis* **28**, 433–440.
84 Raab M, Gentili M, de Belly H, Thiam H-R, Vargas P, Jimenez AJ, Lautenschlaeger F, Voituriez R, Lennon-Dumenil A-M, Manel N *et al.* (2016) ESCRT III repairs nuclear envelope ruptures during cell migration to limit DNA damage and cell death. *Science* **352**, 359–362.

85 Liu S, Kwon M, Mannino M, Yang N, Renda F, Khodjakov A & Pellman D (2018) Nuclear envelope assembly defects link mitotic errors to chromothripsis. *Nature* **561**, 551–555.
86 Dey D, Dahl J, Cho S & Benjamin TL (2002) Induction and bypass of p53 during productive infection by polyomavirus. *J Virol* **76**, 9526–9532.
87 Justice JL, Needham JM & Thompson SR (2019) BK Polyomavirus Activates the DNA Damage Response To Prolong S Phase. *J Virol* **93**, e00130–19, /jvi/93/14/JVI.00130-19.atom.
88 Huerfano S, Žíla V, Bouřa E, Španielová H, Štokrová J & Forstová J (2010) Minor capsid proteins of mouse polyomavirus are inducers of apoptosis when produced individually but are only moderate contributors to cell death during the late phase of viral infection. *FEBS J* **277**, 1270–1283.
89 Verma S, Ziegler K, Ananthula P, Co JKG, Frisque RJ, Yanagihara R & Nerurkar VR (2006) JC virus induces altered patterns of cellular gene expression: Interferon-inducible genes as major transcriptional targets. *Virology* **345**, 457–467.
90 An P, Sáenz Robles MT, Duray AM, Cantalupo PG & Pipas JM (2019) Human polyomavirus BKV infection of endothelial cells results in interferon pathway induction and persistence. *PLoS Pathog* **15**, e1007505.
91 Horníková L, Žíla V, Španielová H & Forstová J (2015) Mouse polyomavirus: propagation, purification, quantification, and storage. *Curr Protoc Microbiol* **38**, 14F.1.1–14F.1.26.
92 Nabbi A & Riabowol K (2015) Rapid isolation of nuclei from cells *in vitro*. *Cold Spring Harb Protoc* **2015**, pdb.prot083733.
93 Solovei I & Cremer M (2010) 3D-FISH on cultured cells combined with immunostaining. In Fluorescence *in situ* Hybridization (FISH) (Bridger JM & Volpi EV, eds), pp. 117–126.Humana Press, Totowa, NJ.